2014

Development of the Single-Relaxation-Time Lattice Boltzmann Method for Application to Thermal Fluid Flows

Gregory Scott
Lehigh University

Development of the Single-Relaxation-Time Lattice Boltzmann Method

for Application to Thermal Fluid Flows

by

Gregory Scott

A Thesis

Presented to the Graduate and Research Committee

of Lehigh University

in Candidacy for the Degree of

Master of Science

in

Mechanical Engineering

Lehigh University

December 2014

Copyright Page

Thesis Signature Sheet

This thesis is accepted and approved in partial fulfillment of the requirements for the

Master of Science.

_____
Date Approved

_____
Dr. Alparslan Oztekin, Thesis Advisor

_____
Dr. Gary Harlow, Chairperson
Mechanical Engineering and Mechanics

Acknowledgments

Table of Contents

List of Figures

Abstract

This work investigates the single-relaxation-time Lattice Boltzmann Method and how to develop it into a full hydrodynamic and thermal modeling scheme. First the single-relaxation time isothermal Lattice Boltzmann Method is outlined, beginning with the fundamentals of the lattice model and then proceeding through the necessary governing equations for the two-dimensional, nine-directional lattice. The governing equations are then presented in a discretized form to be used for simulation, followed by treatment of boundary conditions. Fluid and dimensional properties are explained in terms of both lattice units and physical units via conversion factors. Next is an introduction to thermal Lattice Boltzmann, discussing the changes as well as going through new governing equations pertaining to the internal energy density distribution function. Then the thermal scheme is shown in discretized form along with thermal boundary conditions and updated hydrodynamic boundary conditions. Fluid properties are reviewed alongside thermal properties, as they are essential to know when designing a simulation. Finally, results are shown for some two-dimensional channel flow geometries with hot and cold surfaces: a uniform-width channel, a channel that undergoes sudden expansion, and a channel featuring sudden contraction. The flow within the channel could be dominated by the density stratification or the forced flow introduced at the inlet. These mixed flows of natural and forced convection are characterized by the Reynolds and Rayleigh numbers, the Rayleigh numbers above critical value to allow for formation of natural convection

cells when experiencing low-Reynolds flows. The results are presented as contour plots of temperature and stream function.

Introduction

The Lattice Boltzmann Method (LBM) is a numerical method for fluid simulation with a relatively young history, not gaining popularity until the 1990's. The backbone of LBM is the Boltzmann Equation, which dictates particle transportation on a microscopic level, but can be used to find macroscopic quantities such as the velocity or temperature fields of a moving fluid. LBM is considered a modern descendant of the Lattice Gas Automata Method (or HPP Method) developed by Hardy, Pomeau and De Pazzis in the 1970's which modeled the streaming and collision process of discrete particles as they moved amongst each other **[Hardy, 1976]**. The primary improvement of LBM over the HPP Method is that LBM no longer manages a large quantity of individual particles, but instead works in terms of a density distribution function that represents the number of particles per unit volume that are travelling in each direction along a lattice **[Succi, 1991]**. Interest in LBM soon grew as it was found to provide accurate results just as efficiently as pre-existing computational schemes such as spectral methods **[Martínez, 1994; Hou, 1995]**.

Early attempts at a thermal model, for scenarios involving heat transfer, included that of a multispeed approach and a passive-scalar approach. The goal of the multispeed approach was to get a thermal evolution equation using only the density distribution, but this

required accounting for higher-order velocity terms and also had a relatively narrow range of numerical stability **[Alexander, 1993; McNamara, 1995]**. On the other hand, the passive-scalar approach worked under the assumption that both viscous heating and compression work were negligible, and thus the temperature could be modeled by evolving a separate distribution function independent of the typical density distribution function. Although these assumptions gave it a limited range of use, it proved to be accurate within this range while maintaining better numerical stability compared to the multispeed approach **[Bartoloni, 1993; Shan, 1997; Eggels, 1995]**.

The search was on for a thermal method that could account for viscous heating and compression work while achieving a wide range of stability. After further derivation of the Boltzmann Equation, an expression for the internal energy distribution was found that could be used as a discretized evolution equation, capable of accounting for all heat transfer while still possessing the same amount of numerical stability and similar execution to the passive-scalar approach **[He, 1997 a; Abe, 1997]**. This discovery was soon put to work and used to tackle some benchmark problems such as thermal Couette flow and Rayleigh-Bénard convection **[He, 1998]**.

The subsequent sections will describe the original single-relaxation-time Lattice Boltzmann Method made purely for hydrodynamic modeling, followed by an explanation of the He-Chen-Doolen adaptation that accounts for full hydrodynamic and thermal flow.

The Single-Relaxation-Time Lattice Boltzmann Method

The Lattice Model

LBM simulations operate on a discretized lattice structure of nodes. The lattice can be described using a naming system that consists of two properties: the dimensions of the lattice, and the number of directions to be considered at each node. This thesis shall cover problems conducted on square grid arrangements under a D2Q9 architecture, meaning two-dimensional lattices with nine directions analyzed at each node. For two-dimensional simulations, D2Q9 is the most commonly used configuration and is shown below in Figure 1.
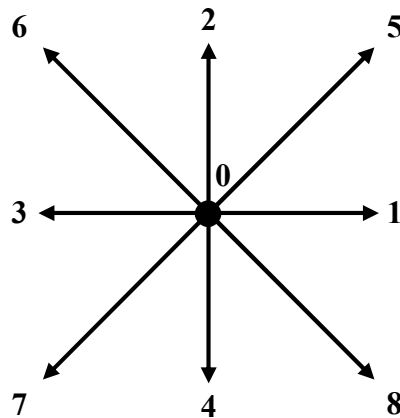
Figure 1 D2Q9 arrangement

The lattice possesses a characteristic lattice speed c. On a square grid, $c = \delta_x/\delta_t$, where δ_x is the orthogonal spacing between lattice nodes and δ_t is the lattice time-step size [**Succi, 2001**]. In many simulations δ_x and δ_t are both chosen to be equal to 1 for the

sake of simplicity. As will be explained later, δ_x and δ_t can take on other values if the goal is to simulate a model with specified physical properties or achieve greater numerical stability when needed. The parameter c_s is known as the lattice sound speed and is equal to $c/\sqrt{3}$.

Governing Equations

The foundation of LBM simulation is the Boltzmann Equation. Expressed in terms of a fluid's single-particle density distribution, this evolution equation is written as

$$\partial_t f + (\boldsymbol{\xi} \cdot \nabla)f = \Omega(f) \tag{1}$$

where f is the particle density distribution, $\boldsymbol{\xi}$ is the microscopic (particle) velocity, and Ω is the collision operator. The distribution function f represents the particles per unit volume that possess a microscopic velocity between $\boldsymbol{\xi}$ and $\boldsymbol{\xi} + \mathrm{d}\boldsymbol{\xi}$. Then the macroscopic density ρ and bulk velocity $\boldsymbol{u}$ are calculated using the first and second moments of f

$$\rho = \int f \, \mathrm{d}\boldsymbol{\xi} \tag{2}$$

$$\rho\boldsymbol{u} = \int \boldsymbol{\xi} f \, \mathrm{d}\boldsymbol{\xi} \tag{3}$$

The collision term Ω is a rather complex term, and for most common purposes can be replaced with a single-relaxation-time approximation. This style of LBM is referred to as single-relaxation-time LBM, or SRTLBM. The collision approximation is known as the Bhatnagar-Gross-Krook (BGK) model **[Bhatnagar, 1954]**

$$\Omega(f) = -\frac{f - f^{eq}}{\tau} \tag{4}$$

The constant τ is the relaxation time of the model and f^{eq} is the equilibrium distribution function. In general form, the equilibrium distribution is expressed as a Maxwell-Boltzmann distribution

$$f^{eq} = \frac{\rho}{(2\pi RT)^{D/2}} e^{\frac{-(\boldsymbol{\xi}-\boldsymbol{u})^2}{2RT}} \tag{5}$$

Here, R is the gas constant, T is the temperature, and D is the dimension of the model. In isothermal LBM, the product RT is simply equal to $c^2/3$. More information on these governing equations can be found in the work of He and Luo **[He, 1997 b]**.

Discretized Equations

Combining equations (1) and (4), the discretized evolution equation is represented as

$$f(\boldsymbol{x} + \boldsymbol{e}\delta_t, t + \delta_t) - f(\boldsymbol{x}, t) = -\frac{1}{\tau}[f(\boldsymbol{x}, t) - f^{eq}(\boldsymbol{x}, t)] \tag{6}$$

where t is the current lattice time and $\boldsymbol{e}$ is the lattice microscopic velocity vector. It should be noted here that for the D2Q9 arrangement (Fig. 1), both f and $\boldsymbol{e}$ are each split into 9 directional components which shall be denoted as $0 \le k \le 8$. The full vector $\boldsymbol{e}$ is then

$$\boldsymbol{e} = \begin{Bmatrix} 0 & c & 0 & -c & 0 & c & -c & -c & c \\ 0 & 0 & c & 0 & -c & c & c & -c & -c \end{Bmatrix} \tag{7}$$

where each column represents $\boldsymbol{e}_k$, the x- and y-components for a single direction k.

Similarly, each direction of f is written as f_k and essentially represents the particles per

unit volume travelling in the direction k. Since SRTLBM is a completely explicit

method, and each direction k is calculated individually at each node during simulation,

the discretized evolution equation can be more appropriately expressed as

$$f_k(\boldsymbol{x} + \boldsymbol{e}_k\delta_t, t + \delta_t) = f_k(\boldsymbol{x}, t) - \frac{1}{\tau}\left[f_k(\boldsymbol{x}, t) - f_k^{eq}(\boldsymbol{x}, t)\right] \tag{8}$$

Note that equation (8) will not work for some directions of f_k along boundaries, as it

would require knowing f_k at a non-fluid node. The next section will describe boundary

conditions that can be applied at such nodes in order to update values for the remaining

f_k there. Once all f_k have been calculated at all nodes for the current iteration, the density

ρ and bulk velocity $\boldsymbol{u}$ can then be updated at each node:

$$\rho = \sum_k f_k \tag{9}$$

$$\rho\boldsymbol{u} = \sum_k \boldsymbol{e}_k f_k \tag{10}$$

Now the only variable left to update before the next time-step is f^{eq} for each node in

each direction k. The discretized form of f_k^{eq} is represented by the Chapman-Enskog

expansion

$$f_k^{eq} = w_k\rho\left[1 + 3\frac{\boldsymbol{e}_k \cdot \boldsymbol{u}}{c^2} + \frac{9}{2}\frac{(\boldsymbol{e}_k \cdot \boldsymbol{u})^2}{c^4} - \frac{3}{2}\frac{\boldsymbol{u}^2}{c^2}\right] \tag{11}$$

where w_k is a direction-based weighting coefficient **[Succi, 2001]**

$$w = \left\{ \frac{4}{9} \quad \frac{1}{9} \quad \frac{1}{9} \quad \frac{1}{9} \quad \frac{1}{9} \quad \frac{1}{36} \quad \frac{1}{36} \quad \frac{1}{36} \quad \frac{1}{36} \right\} \tag{12}$$

With new values of f^{eq} everywhere, the time-step is now increased and the simulation continues on to the next iteration.

Hydrodynamic Boundary Conditions

There are many boundary nodes within a lattice where equation (8) cannot be used to solve for f_k in all directions, as certain directions would depend on nodes in which there is no fluid (a solid wall boundary, for example). Using periodic boundaries bypasses this problem, as the unknown directions for a node on one boundary are simply equal to the known directions for the corresponding node on the opposite boundary. For all other boundaries where either the density or velocity is known, equations (9) and (10) still hold true and can be useful for such situations. Expanding equations (9) and (10), as well as separating equation (10) into an x-component relation and y-component relation, leads to three equations at one's disposal:

$$\rho = f_0 + f_1 + f_2 + f_3 + f_4 + f_5 + f_6 + f_7 + f_8 \tag{13}$$

$$\rho \frac{u_x}{c} = f_1 + f_5 + f_8 - f_3 - f_6 - f_7 \tag{14}$$

$$\rho \frac{u_y}{c} = f_2 + f_5 + f_6 - f_4 - f_7 - f_8 \tag{15}$$

In most cases, the above three equations are insufficient when trying to solve for the unknown f_k's, especially since the node's density or velocity may be unknown as well. He and Zou developed a simple way to remedy this by assuming that the non-equilibrium part of the density distribution normal to the boundary will bounce back in the opposite direction **[Zou, 1997]**. In other words, for two opposing directions α and β at a boundary node:

$$f_\alpha - f_\alpha^{eq} = f_\beta - f_\beta^{eq} \tag{16}$$

This non-equilibrium bounce-back is a widely-used condition and works very well in most places. For instance, consider a node along the top solid wall of a two-dimensional channel. Assuming a stationary no-slip boundary, both u_x and u_y must be zero. After evolution using equation (8), the remaining unknowns are f_4, f_7, f_8, and ρ. Applying the non-equilibrium bounce-back normal to the wall gives $f_4 - f_4^{eq} = f_2 - f_2^{eq}$. Since u_x and u_y are both zero, $f_4^{eq} = f_2^{eq}$ and thus $f_4 = f_2$. Equations (13), (14), and (15) can then be solved to obtain f_7, f_8, and ρ.

Another common boundary condition is a specified density or velocity at an opening such as an inlet or outlet. For example, take the case of a two-dimensional channel once again, this time focusing on a node along the inlet on the left end. Suppose that the velocity is specified as $u_x = U$ and $u_y = 0$, making the unknowns f_1, f_5, f_8, and ρ. The non-

equilibrium bounce-back condition states that $f_1 = f_3 - (f_3^{eq} - f_1^{eq})$, this time resulting

in $f_1 = f_3 + \frac{2}{3}\rho\frac{U}{c}$. Combine this with equations (13-15) to solve for the four unknowns.

Corner nodes can be solved in a very similar fashion. Now consider the upper-left corner of the same channel, where the inlet meets the top wall. Since this corner node is technically along the top wall, the no-slip condition dictates that u_x and u_y are zero. The unknown variables are f_1, f_4, f_5, f_7, f_8, and ρ. Non-equilibrium bounce-back can be applied in both the horizontal and vertical directions, since both are normal to a boundary, giving $f_1 = f_3$ and $f_4 = f_2$. Combining this with equations (14) and (15) reveals that $f_5 = f_7$ and $f_8 = f_6$, allowing for solution of the system.

Property Calculation and Relation to Physical Units

When the time comes to run a SRTLBM simulation, there is often a desire to model a specific scenario given non-dimensional parameters or physical properties. The most common non-dimensional quantities specified are the Reynolds number Re and lattice Mach number Ma, each given by

$$Re = \frac{UL}{\nu} \tag{17}$$

$$Ma = \frac{|\boldsymbol{u}|}{c_s} = \sqrt{3}\frac{|\boldsymbol{u}|}{c} \tag{18}$$

where U is the characteristic velocity, L is the characteristic length (for 2D channel flow, this is the height of the channel), and ν is the kinematic viscosity. In lattice units, the

channel height L is really the number of nodes spanning across the channel multiplied by

δ_x, since δ_x is the "lattice distance" between each node, resulting in a lattice-unit length.

The kinematic viscosity given in terms of lattice units **[He, 1997 b]** is

$$v = \left(\tau - \frac{1}{2}\right) c_s^2 \delta_t = \frac{(2\tau - 1)}{6} \frac{\delta_x^2}{\delta_t} \tag{19}$$

Please note that a slightly different expression is used for v in the Thermal SRT method

discussed later in this paper. The relaxation time τ has a significant impact on the

stability of the simulation, and must be greater than ½. As long as the simulation is stable,

τ can be selected in order to satisfy the specified constraints; the range for best

performance is typically between 0.6 and 0.8 for isothermal SRTLBM.

For incompressible flow, it is important to keep the Mach number below 0.1 or 0.15 for

accurate results. This is another constraint to keep in mind when setting up a simulation.

All in all, the goal of running a successful simulation in the least amount of time is to

model the designated Reynolds number while using the smallest node grid possible,

while making sure that τ is within a stable range and the flow is incompressible

throughout the domain.

Since all SRTLBM variables have been presented in terms of lattice units up to now,

developing a correlation to physical units would prove more meaningful to those

interested in realistic scenarios. Of course, all non-dimensional quantities such as the

Reynolds number still hold whether expressed in lattice units or physical units. Thus one

useful relationship is $\frac{UL}{\nu} = \frac{U_p L_p}{\nu_p}$, where the left side is the Reynolds number in terms of

lattice quantities and the right-hand side in terms of physical quantities. To differentiate

between lattice and physical units in this work, the author will designate all physical

quantities with the subscript p. The characteristic length L_p is divisible by the number of

node spaces along its characteristic direction to give $\delta_{x,p}$, the representative physical

spacing between each node in the square lattice. One can then define a length conversion

factor $L_0 = \frac{\delta_{x,p}}{\delta_x}$ [Llewellin, 2010; Latt, 2008]. Using a time conversion factor $t_0 = \frac{\delta_{t,p}}{\delta_t}$

as the ratio of actual time passing between each time-step to "lattice time" between each

step also proves beneficial. These form a relationship between the viscosities, $\nu_p = \frac{L_0^2}{t_0}\nu$,

as well as a relationship between the characteristic velocities, $U_p = \frac{L_0}{t_0}U$. In addition, a

mass conversion factor M_0 can be conceived such that $\rho_p = \frac{M_0}{L_0^3}\rho$. These unit conversion

relations make it possible to set up a simulation by first selecting a particular set of

desired physical properties, then deriving the necessary lattice parameters to use during

execution. If the chosen parameter set does not produce a stable simulation, then the user

will have to adjust elements such as the number of nodes, time-step size, and node

spacing.

Thermal SRTLBM: The Novel Thermal Model

Introduction to Thermal LBM

The proceeding explanation of thermal LBM will follow the "novel thermal model" scheme proposed by He, Chen, and Doolen **[He, 1998]**. The foundation of this method is to introduce a second distribution function g, which is the internal *energy* density distribution within the lattice. The function g shares the same dimensions and directions as f, and undergoes evolution similar to f. Some other changes occur due to the fact that the model is no longer isothermal; for instance, the lattice speed and lattice sound speed, c and c_s, will now vary at each node as they are dependent on the local temperature. This means that the microscopic velocity vector e can also vary throughout the lattice now as it is dependent on c. The lattice speed c at a node is $c = \sqrt{3RT}$ and the sound speed is $c_s = \sqrt{RT}$, where R is the gas constant and T is the node's local temperature. The relationship to the constants δ_x and δ_t still exists as $c_{char} = \frac{\delta_x}{\delta_t}$, where c_{char} is the characteristic lattice speed defined by a characteristic temperature T_{char}:

$$c_{char} = \frac{\delta_x}{\delta_t} = \sqrt{3RT_{char}} \tag{20}$$

Likewise, the characteristic sound speed is $c_{s,char} = \sqrt{RT_{char}}$. The characteristic quantities play an important role in setting up parameters for a thermal simulation, to be discussed later on; the following is an explanation of the thermal method itself.

Governing Equations

In thermal LBM, the evolution equation defined in equation (1) still holds for the particle

density distribution f, but now with the addition of an external force term F:

$$\partial_t f + (\boldsymbol{\xi} \cdot \nabla)f = \Omega(f) + F \tag{21}$$

The force term F is based on $\boldsymbol{G}$, a vector signifying the external force per unit mass:

$$F = \frac{\boldsymbol{G} \cdot (\boldsymbol{\xi} - \boldsymbol{u})}{RT} f^{eq} \tag{22}$$

Taking the first and second moments of F gives $\int F d\boldsymbol{\xi} = 0$ and $\int F\boldsymbol{\xi} d\boldsymbol{\xi} = \rho\boldsymbol{G}$,

respectively. The relaxation time τ_f for evolution of f is now designated with a subscript

because there is a separate relaxation time τ_g for the evolution of g.

The assumption of a constant collision operator in the BGK approximation produces a

second-order truncation error. Normally the viscosity ν is given by $\nu = \tau_f RT$ but

modifying this relationship into equation (19) absorbs this error for isothermal LBM. In

thermal LBM however, viscosity plays a part in the energy evolution as well via a

viscous heating term. This viscous heating term is based on a simpler first-order

approximation of the Boltzmann Equation and thus does not experience the same second-

order truncation error, so the viscosity must remain $\nu = \tau_f RT$ for viscous heating. A

technique used to address the truncation error without modifying the viscosity equation

above is to perform a second-order temporal integration on the Boltzmann Equation to

form a new evolution equation for f:

14

$$f(x + \xi\delta_t, \xi, t + \delta_t) - f(x, \xi, t)$$

$$= -\frac{\delta_t}{2\tau_f}[f(x + \xi\delta_t, \xi, t + \delta_t) - f^{eq}(x + \xi\delta_t, \xi, t + \delta_t)]$$

$$-\frac{\delta_t}{2\tau_f}[f(x, \xi, t) - f^{eq}(x, \xi, t)] + \frac{\delta_t}{2}F(x + \xi\delta_t, \xi, t + \delta_t) + \frac{\delta_t}{2}F(x, \xi, t)$$

(23)

This new version of the density evolution is both long-winded and implicit, but a quick substitution solves both of these issues:

$$\bar{f} = f + \frac{\delta_t}{2\tau_f}(f - f^{eq}) - \frac{\delta_t}{2}F$$

(24)

The $\bar{f}$ substitution produces the more manageable density evolution equation:

$$\bar{f}(x + \xi\delta_t, \xi, t + \delta_t) - \bar{f}(x, \xi, t)$$

$$= -\frac{\delta_t}{\tau_f + \delta_t/2}[\bar{f}(x, \xi, t) - f^{eq}(x, \xi, t)] + \frac{\tau_f\delta_t}{\tau_f + \delta_t/2}F(x, \xi, t)$$

(25)

On the other hand, the derivation of the *energy* density distribution begins by going another step beyond equations (2) and (3) and now taking the third moment of f:

$$\frac{\rho DRT}{2} = \int \frac{(\xi - u)^2}{2}f\mathrm{d}\xi$$

(26)

Again, D is the dimension of the lattice (two-dimensional for this thesis), R is the gas constant, and T is the local temperature. The internal energy density distribution g is then defined to be

$$g = \frac{(\boldsymbol{\xi} - \boldsymbol{u})^2}{2} f \tag{27}$$

so that

$$\frac{\rho DRT}{2} = \int g \, \mathrm{d}\boldsymbol{\xi} \tag{28}$$

The Boltzmann Equation adjusted to represent the evolution of g is

$$\partial_t g + (\boldsymbol{\xi} \cdot \nabla)g = \frac{(\boldsymbol{\xi} - \boldsymbol{u})^2}{2} \Omega(f) - fq \tag{29}$$

where the collision term can be approximated as

$$\frac{(\boldsymbol{\xi} - \boldsymbol{u})^2}{2} \Omega(f) = -\frac{g - g^{eq}}{\tau_g} \tag{30}$$

and the equilibrium energy distribution is

$$g^{eq} = \frac{\rho(\boldsymbol{\xi} - \boldsymbol{u})^2}{2(2\pi RT)^{D/2}} e^{\frac{-(\boldsymbol{\xi}-\boldsymbol{u})^2}{2RT}} = \frac{(\boldsymbol{\xi} - \boldsymbol{u})^2}{2} f^{eq} \tag{31}$$

The term fq on the right-hand side of equation (29) represents viscous heat dissipation, where

$$q = (\boldsymbol{\xi} - \boldsymbol{u}) \cdot [\partial_t \boldsymbol{u} + (\boldsymbol{\xi} \cdot \nabla)\boldsymbol{u}] \tag{32}$$

although the problems presented in this paper will neglect the effects of viscous heating.

The evolution equation for g undergoes the same time-wise integration that created equation (23). The result is very similar to (23) and also requires a substitution in order to maintain explicitness:

16

$$\bar{g} = g + \frac{\delta_t}{2\tau_g}(g - g^{eq}) + \frac{\delta_t}{2}fq \tag{33}$$

Substituting in $\bar{g}$ produces an energy evolution equation in terms of $\bar{g}$:

$$\bar{g}(x + \xi\delta_t, \xi, t + \delta_t) - \bar{g}(x, \xi, t)$$

$$= -\frac{\delta_t}{\tau_g + \delta_t/2}[\bar{g}(x, \xi, t) - g^{eq}(x, \xi, t)] - \frac{\tau_g\delta_t}{\tau_g + \delta_t/2}f(x, \xi, t)q(x, \xi, t) \tag{34}$$

where τ_g is the relaxation time for the energy density collision operator.

Discretized Equations

From equation (25), the discretized evolution of $\bar{f}$ is

$$\bar{f}_k(x + e_k\delta_t, t + \delta_t)$$

$$= \bar{f}_k(x, t) - \frac{\delta_t}{\tau_f + \delta_t/2}[\bar{f}_k(x, t) - f_k^{eq}(x, t)] + \frac{\tau_f\delta_t}{\tau_f + \delta_t/2}F_k(x, t) \tag{35}$$

and from (34) the discretized evolution of $\bar{g}$ is

$$\bar{g}_k(x + e_k\delta_t, t + \delta_t)$$

$$= \bar{g}_k(x, t) - \frac{\delta_t}{\tau_g + \delta_t/2}[\bar{g}_k(x, t) - g_k^{eq}(x, t)] - \frac{\tau_g\delta_t}{\tau_g + \delta_t/2}f_k(x, t)q_k(x, t) \tag{36}$$

The particle velocity vector e still follows its definition given by equation (7), except that

the lattice speed c is no longer a constant throughout the lattice and is now dependent on

the local node temperature: $c = \sqrt{3RT}$.

17

The directional force F_k is dependent on $\boldsymbol{G}$, the external force per unit mass. In the following study, $\boldsymbol{G}$ is the buoyancy force based on the Boussinesq approximation

$$\boldsymbol{G} = g_0\beta(T - T_m)\boldsymbol{j} \tag{37}$$

where g_0 is gravitational acceleration, β is the coefficient of thermal expansion, T_m is the characteristic temperature, and $\boldsymbol{j}$ is the unit vector in the direction opposing gravity. Then the directional force F_k is represented by

$$F_k = \frac{\boldsymbol{G} \cdot (\boldsymbol{e}_k - \boldsymbol{u})}{RT} f_k^{eq} \tag{38}$$

Note that the viscous heating term fq in equation (36) is based on f and not $\bar{f}$. If the inclusion of viscous heat effects is necessary for a simulation, then f can be calculated by simply reversing the substitution introduced in equation (24):

$$f_k = \frac{\tau_f \bar{f}_k + \frac{\delta_t}{2} f_k^{eq} + \frac{\tau_f \delta_t}{2} F_k}{\tau_f + \frac{\delta_t}{2}} \tag{39}$$

The second component of the viscous heat dissipation term, q, is

$$q = (\boldsymbol{e}_k - \boldsymbol{u}) \cdot [\partial_t \boldsymbol{u} + (\boldsymbol{e}_k \cdot \nabla)\boldsymbol{u}] \tag{40}$$

which will require the partial derivatives $\partial_t \boldsymbol{u}$, $\partial_x \boldsymbol{u}$, and $\partial_y \boldsymbol{u}$ for 2D simulation. These can be calculated each time-step by using an approximation technique like finite differencing.

The density ρ, bulk velocity $\boldsymbol{u}$, and temperature T of a node are then respectively

18

$$\rho = \sum_k \bar{f}_k \tag{41}$$

$$\rho \boldsymbol{u} = \sum_k \boldsymbol{e}_k \bar{f}_k + \frac{\rho \boldsymbol{G} \delta_t}{2} \tag{42}$$

$$\frac{\rho DRT}{2} = \sum_k \bar{g}_k - \frac{\delta_t}{2} \sum_k f_k q_k \tag{43}$$

The last required calculation for the time-step is the determination of f^{eq} and g^{eq}. This can be done easily by calculating all directions of f^{eq} using equation (11) which still holds true for thermal LBM, then finding g^{eq} as

$$g_k^{eq} = \frac{(\boldsymbol{e}_k - \boldsymbol{u})^2}{2} f_k^{eq} \tag{44}$$

Hydrodynamic and Thermal Boundary Conditions

Thermal LBM simulation requires both hydrodynamic and thermal boundary conditions. Fortunately, the hydrodynamic boundary conditions developed for isothermal LBM earlier still apply. Equations (13-16) are still functional except for one slight difference: the y-component balance of equation (15) would now have the term $\frac{\rho G \delta_t}{2}$ added to the end. This is due to buoyancy modifying the y-direction of the velocity field as seen in equation (42).

The approach for thermal boundary conditions described here is rather straightforward guess-correction method **[Liu, 2010]**. The first step is to specify the desired local boundary temperature T_b. For boundaries where the condition is not constant-

19

temperature, then T_b can be determined through an approximation based on surrounding nodes in such a way to satisfy the condition. Next, a preliminary guess T^* for node temperature is made by using equation (43) and replacing each unknown $\bar{g}_k$ direction with a guess value $\bar{g}_k^*$. Then define a correction factor G_c as

$$G_c = \frac{\rho DR}{2} \frac{(T_b - T^*)}{\sum_k w_k} \tag{45}$$

where $\sum_k w_k$ is the sum of the weighting coefficients w_k for each of the unknown $\bar{g}_k$ directions involved. For instance, for a south-side wall with unknown $\bar{g}_k$ in the directions $k = 2,5,6$, then $\sum_k w_k = w_2 + w_5 + w_6$. Corner nodes can be handled the same way but will have more unknown directions to solve for. The final step is to use G_c to correct each of the $\bar{g}_k^*$ guess values:

$$\bar{g}_k = \bar{g}_k^* + w_k G_c \tag{46}$$

There are a few different methods for selecting the initial guesses $\bar{g}_k^*$, all of which have been shown to have negligible differences between each other when used for simulation: $\bar{g}_k^*(\boldsymbol{x}, t) = \bar{g}_k(\boldsymbol{x}, -\boldsymbol{e}_k, t)$, $\bar{g}_k^*(\boldsymbol{x}, t) = \bar{g}_k(\boldsymbol{x}, \boldsymbol{e}_k, t - \delta_t)$, $\bar{g}_k^*(\boldsymbol{x}, t) = g_k^{eq}(\boldsymbol{x}, \boldsymbol{e}_k, t)$, and $\bar{g}_k^*(\boldsymbol{x}, t) = 0$. The author chose to consistently use the condition $\bar{g}_k^*(\boldsymbol{x}, t) = g_k^{eq}$ for this work.

Property Calculation

It is time to revisit useful property relations, but now for thermal LBM. To begin, the Reynolds number and the Mach number shown by equations (17) and (18) still hold as

20

such. However, as explained previously, the kinematic viscosity ν is no longer given by equation (19) but rather by

$$\nu = \tau_f RT \tag{47}$$

Similarly, the coefficient of thermal conductivity χ is

$$\chi = \frac{D+2}{D}\tau_g RT \tag{48}$$

or merely $\chi = 2\tau_g RT$ in two dimensions. This results in a simple expression for the

Prandtl number as $Pr = \frac{\nu}{\chi} = \frac{\tau_f}{2\tau_g}$.

The scenarios presented in this paper will deal with convection-driven situations characterized by their Rayleigh number, given as

$$Ra = \frac{g_0\beta\Delta T L^3}{\nu\chi} \tag{49}$$

where the characteristic length L is the height of the channel and ΔT is the temperature difference between hot and cold surfaces. This is further constrained by using an incompressibility condition, $g_0\beta\Delta T L = 0.1$, suggested by He et al. [He, 1998].

The buoyancy acceleration magnitude is $g_0\beta(T - T_m)$ as seen in equation (37), where the characteristic temperature T_m is the mean temperature between the specified hot and cold surfaces. T_m is also used as the characteristic temperature for obtaining a c_{char}, $c_{s,char}$, and ν_{char}, such that $Re = \frac{UL}{\nu_{char}}$ and $c_{char} = \frac{\delta_x}{\delta_t}$ (see equation 20). In this thermal

scheme, both relaxation times τ_f and τ_g should be at least 0.1 to avoid numerical instability in simulations, not to be confused with the recommendation given earlier for isothermal LBM. Since the constants R and β are always seen in conjunction with T, they are both set to be 1 for all proceeding simulations presented here. This is acceptable since physical properties will not be specified.

Thermal LBM Simulation Results

Benchmark Tests

The time has come to demonstrate some of the capabilities of thermal LBM. To serve as benchmark tests, simulations were performed for two elementary flows: isothermal Poiseuille flow to exhibit purely hydrodynamic behavior, and Rayleigh-Bénard convection to show purely heat-driven convective flow.

The isothermal Poiseuille flow example to be demonstrated here was modeled as a two-dimensional channel of uniform width, with a uniform (characteristic) velocity specified at the inlet and a constant uniform pressure (density ρ) specified at the outlet. Both solid walls are treated with the no-slip bounce-back condition described previously. Shown below in steady-state, a lattice grid size of 300x31 was sufficient to simulate flow with a Reynolds number of 30. Other parameters include: $\delta_x = \delta_t = 1$, $\tau_f = 0.15$, specified $U_{in} = 0.05$, and specified $\rho_{out} = 1$.

Figure 2 shows the streamlines of the modeled Poiseuille flow in steady-state after about

20,000 time-steps, as well as the x-directional velocity profile across the width of the

channel at a location downstream. Two-dimensional Poiseuille flow gives a solved

solution that the maximum velocity U_{max}, occurring through the center of the channel,

should be 1.5 times the average velocity, in this case $1.5 * U_{in}$ or 0.075. The observed

data is $U_{max} = 0.0742$ compared to the accepted value of $U_{max} = 0.075$, giving an error

of just 1.1% even for a relatively low lattice resolution of 300x31.
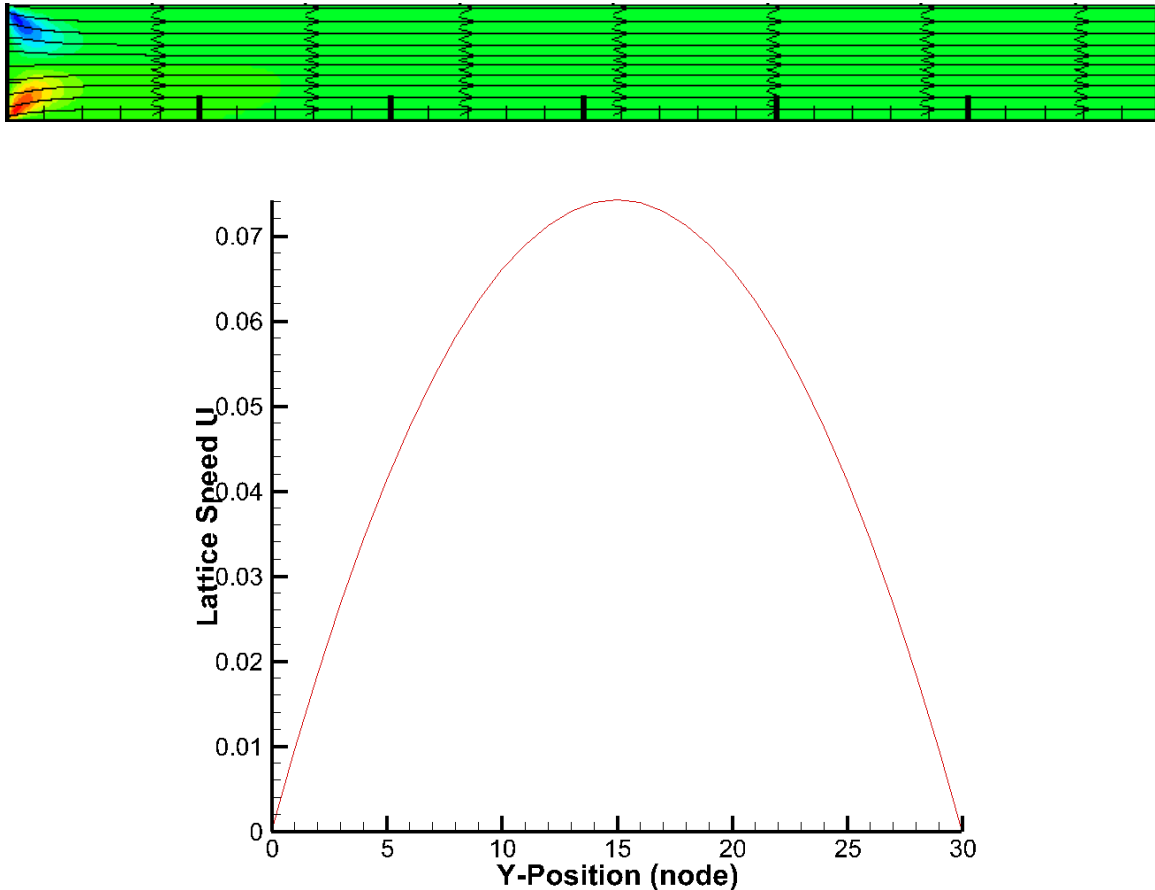
Figure 2 Streamlines and x-directional velocity profile for fully-developed Poiseuille flow at $Re = 30$, $U_{in} = 0.05$

23

The second benchmark test, Rayleigh-Bénard convection, was performed in a channel of the same shape and grid dimensions, but this time with near-zero specified motion. The inlet and top wall have a constant temperature T_{cold} and the bottom wall has a constant temperature T_{hot}. Parameters were chosen to model a Rayleigh number of 3,000 as this is well beyond the critical value of 1707 and should give rise to convection cells. For a channel aspect ratio of 10 such as the one being simulated, there should be enough space for five convection cells to appear, and the results show exactly that. Key parameters include: $\delta_x = \delta_t = 1$, $\tau_g = 0.15$, specified $T_{hot} = 0.38\overline{3}$, $T_{cold} = 0.28\overline{3}$, and $g_0 = 0.0\overline{3}$. The fixed outlet density ρ_{out} is once again set to 1 and will remain so for all future simulations discussed.

See figures 4, 5, and 6 below for temperature, vorticity, and stream function contours, respectively. All temperature contour plots displayed in this paper will show temperatures non-dimensionally as $\frac{T - T_{cold}}{T_{hot} - T_{cold}}$. Also note that stream function values near the inlet of each channel are somewhat distorted due to the boundary condition applied and the method of stream function approximation used there. This is currently being investigated and fortunately has negligible effect on the rest of the channel.

As a side-experiment to see if the critical Rayleigh number could be determined using thermal LBM, prior simulations were run in a smaller channel were a single convection cell was developed with periodic boundary conditions applied to the inlet and outlet. As the Rayleigh number approached the range of 1700-1730, simulation time became a

24

serious burden as it required a larger lattice and a longer runtime to see if any motion

would ever actually occur. Nonetheless, the critical Rayleigh number would fall between

1700 and 1730 according to the thermal LBM trials; this is within about one percent of

the actual value.
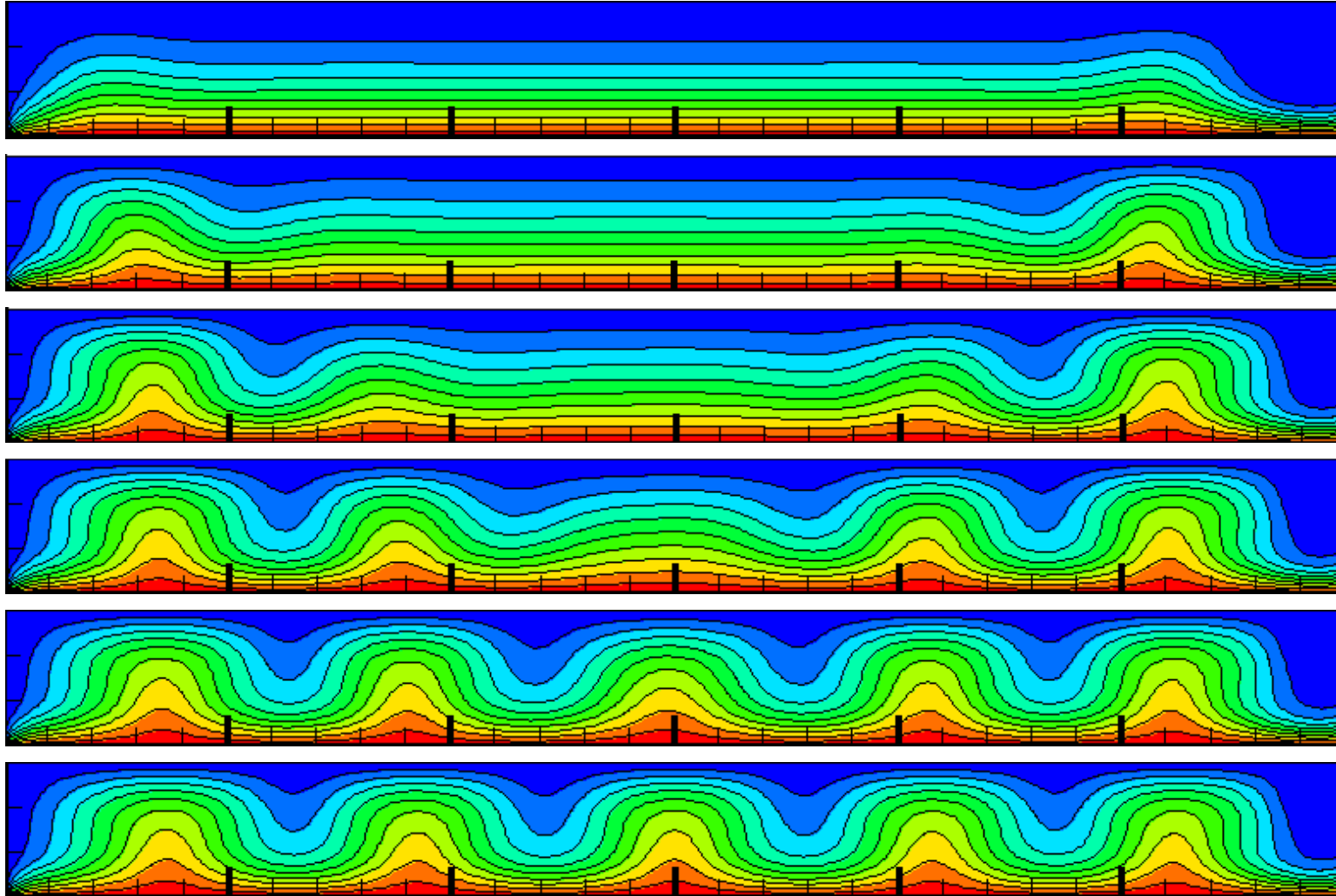
Figure 3 Flat-channel temperature contours for Re $= 0.1$, $Ra = 3000$

at time steps 1000, 2000, 3000, 4000, 5000, and 6000

Vorticity: 3000 and 6000 time steps
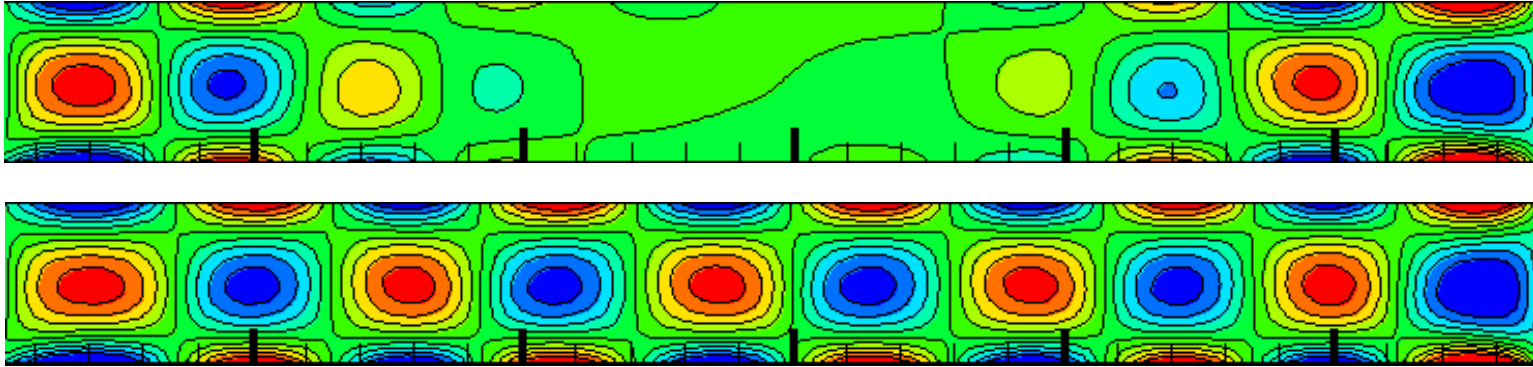
Stream function: 3000 and 6000 time steps
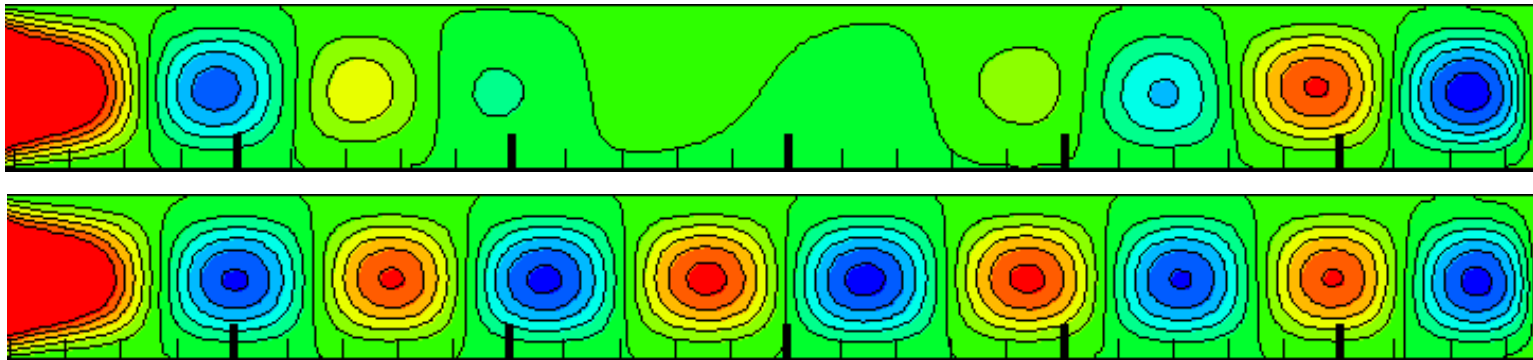
Figure 4 Flat-channel vorticity and stream function contours for Re = 0.1, $Ra = 3000$

Uniform-Width Channel

With verification against elementary flows, now some more interesting flows can be examined with both pressure-driven and heat-driven motion. The first is a revisit of the uniform-width channel as seen in the previous section. Now there is both a specified Reynolds number and specified Rayleigh number. The inlet conditions are a specified uniform velocity U_{in} and constant temperature T_{cold}. The outlet conditions consist of the constant density ρ_{out}, and temperature bounce-back based on a backwards approximation using the previous two nodes. Solid walls are again given no-slip bounce-back; the top wall is fixed at T_{cold} and the bottom wall is fixed at T_{hot}.

The first set of results on this geometry is for $Ra = 3000, Re = 20$. The second set is for $Ra = 3000, Re = 54$. It can be seen that for $Re = 20$, convection cells have more time to develop than at $Re = 54$, but still get swept away by the pressure-driven flow in the channel.

Data from $Re = 20$ are shown below in Figures 5 and 6. The lattice grid size is 1000x101 nodes and key parameters are: $\delta_x = 1$, $\delta_t = 0.5$, $\tau_f = 0.4125$, $\tau_g = 0.22727$, $U_{in} = 0.11$, $g_0 = 0.01$, $T_{hot} = 1.38\bar{3}$, and $T_{cold} = 1.28\bar{3}$.

The data from $Re = 54$ are shown below in Figures 7 and 8. The lattice grid size is 2000x201 nodes and key parameters are: $\delta_x = 1$, $\delta_t = 0.25$, $\tau_f = 0.13\bar{8}$, $\tau_g = 0.16875$, $U_{in} = 0.2$, $g_0 = 0.005$, $T_{hot} = 5.38\bar{3}$, and $T_{cold} = 5.28\bar{3}$.
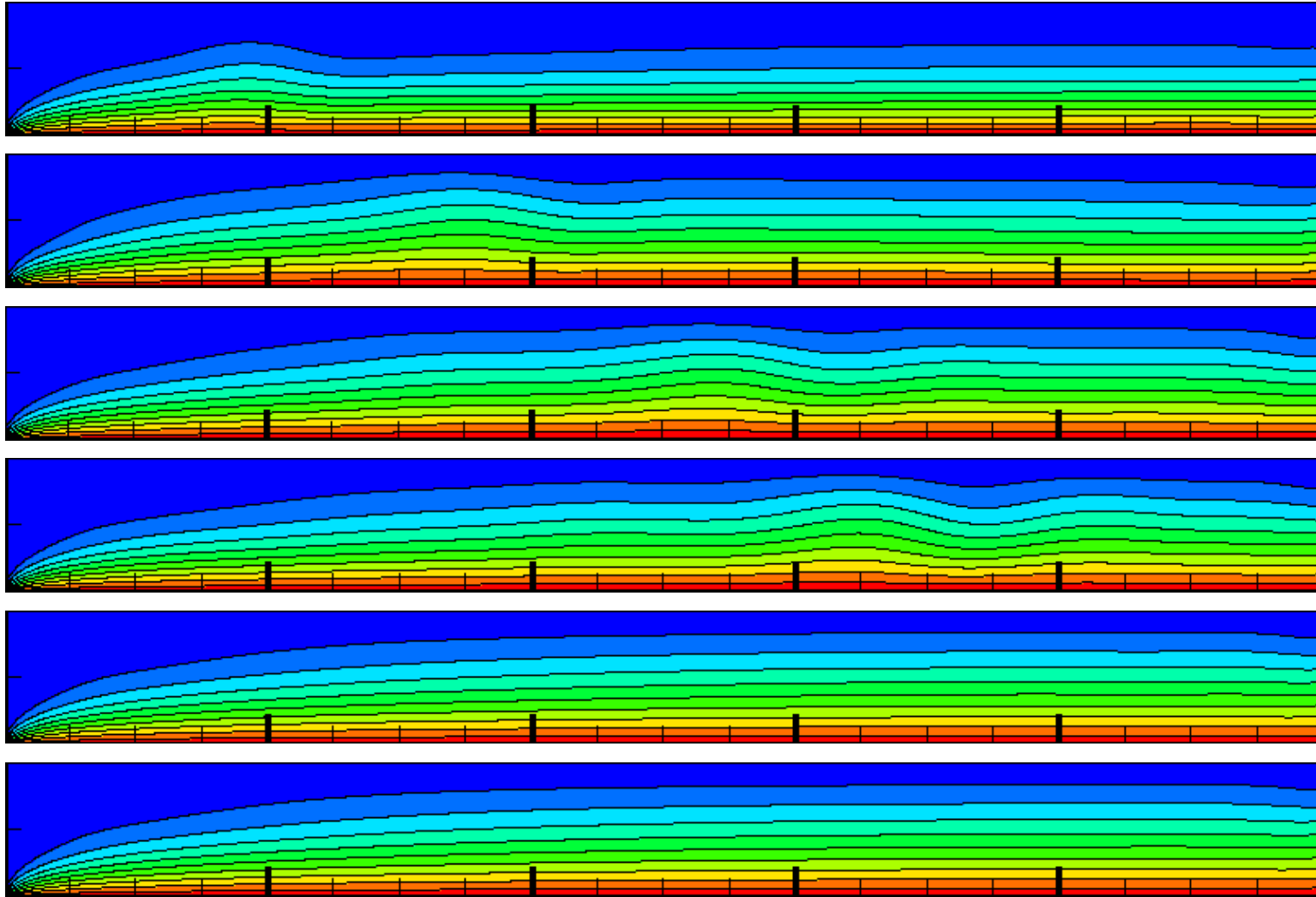
Figure 5 Flat-channel temperature contours for Re = 20, $Ra = 3000$

at time steps 2000, 5000, 10000, 15000, 20000, and 30000
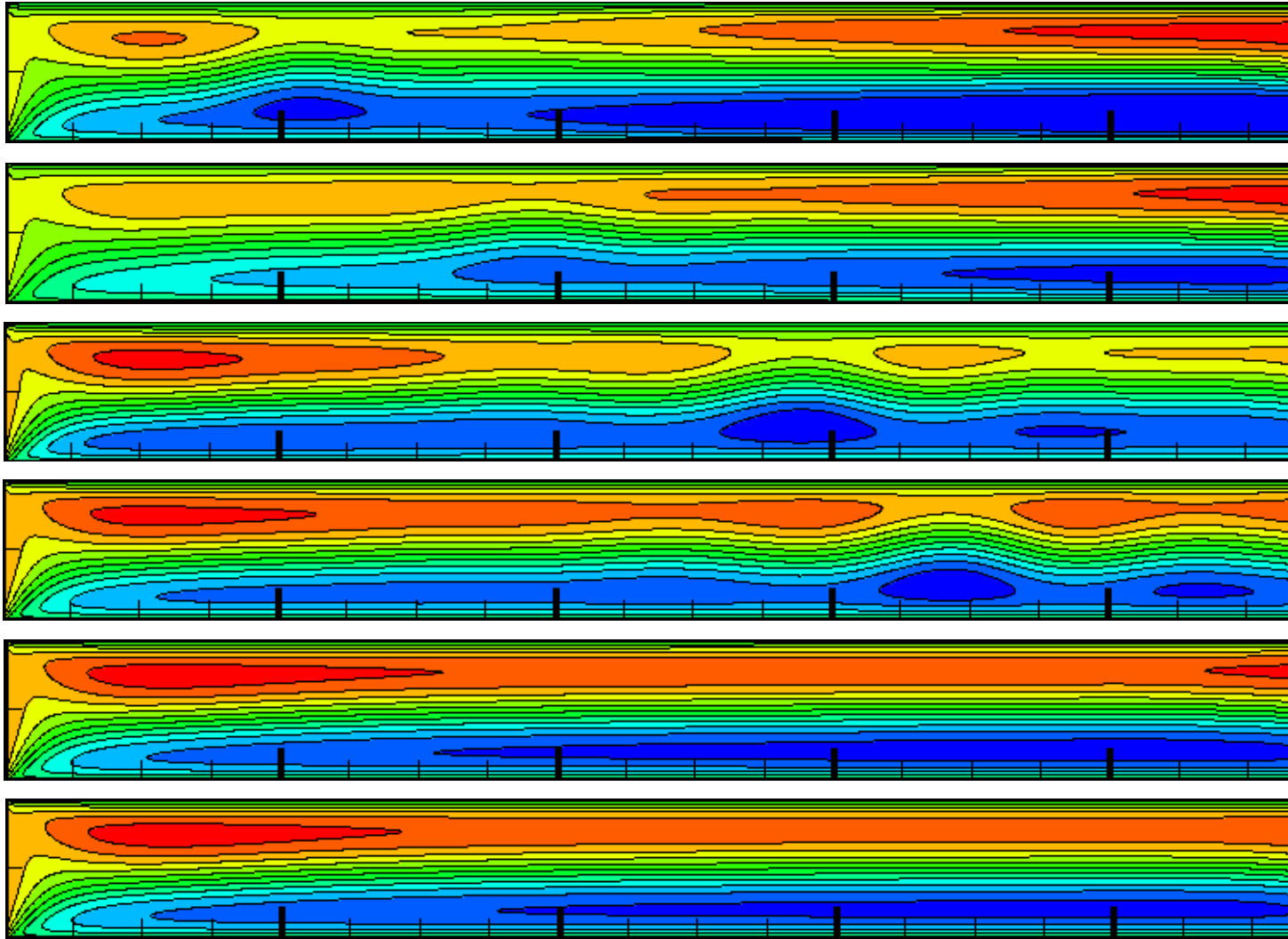
Figure 6 Flat-channel stream function contours for Re $= 20$, $Ra = 3000$

at time steps 2000, 5000, 10000, 15000, 20000, and 30000

30
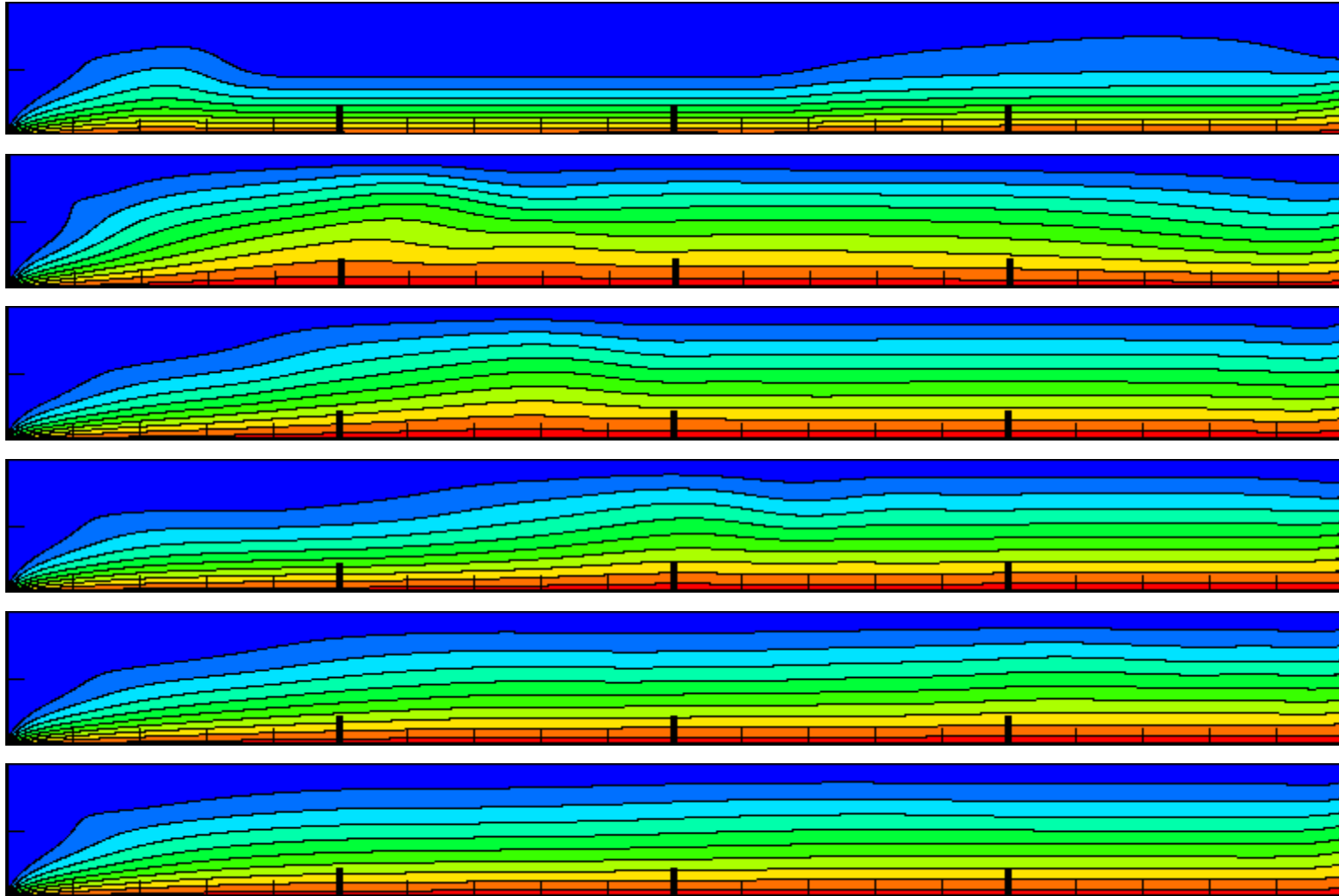
Figure 7 Flat-channel temperature contours for Re $= 54$, $Ra = 3000$

at time steps 5000, 10000, 15000, 20000, 30000, and 40000

31
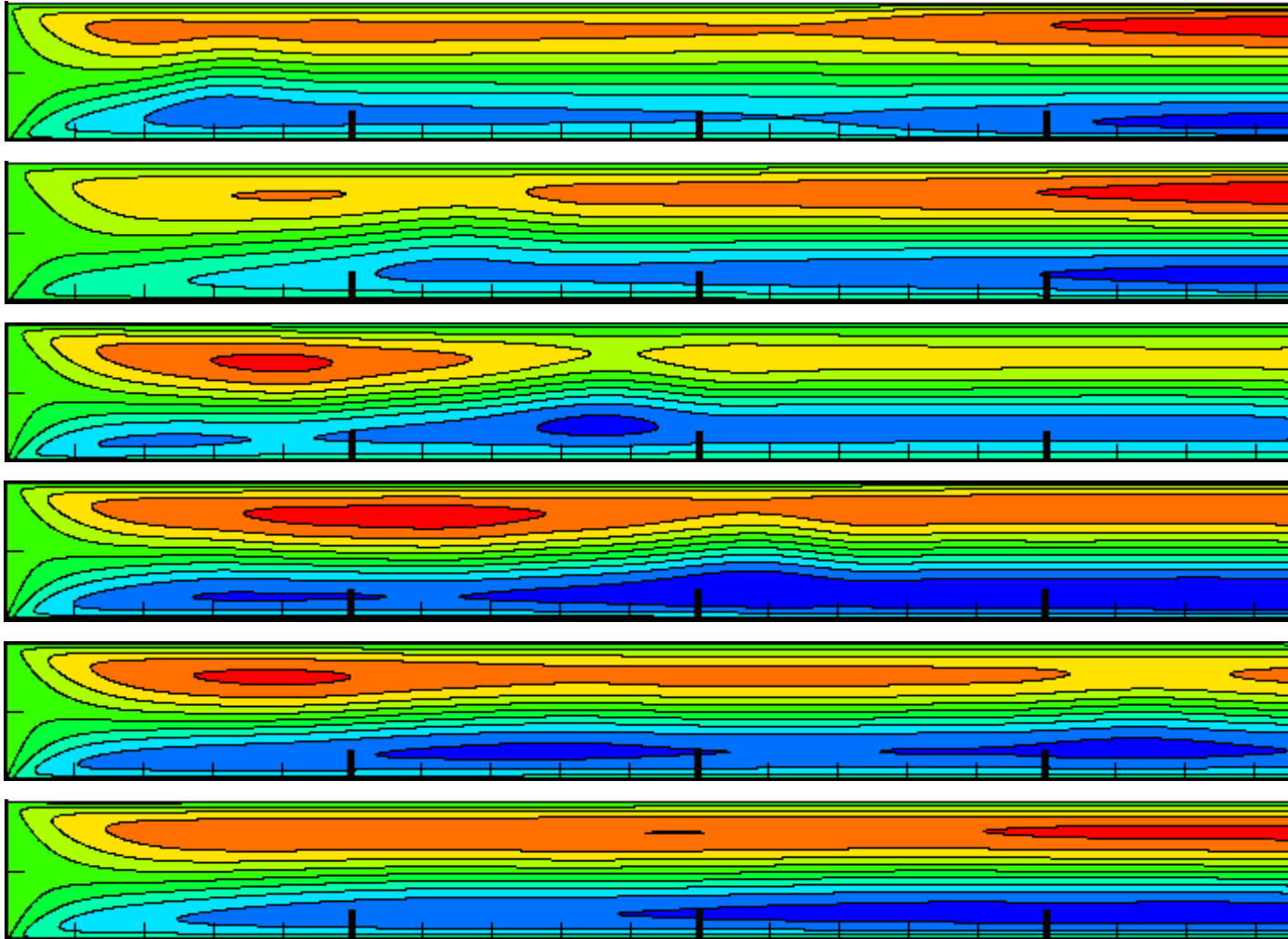
Figure 8 Flat-channel stream function contours for Re = 54, $Ra = 3000$

at time steps 5000, 10000, 15000, 20000, 30000, and 40000

32

Channel with Sudden Expansion

The next geometry to be studied is that of a channel that suddenly doubles in width at a position 40% downstream. The top wall is to remain straight and level with constant temperature T_{cold} while the bottom wall undergoes the change in height. The entire bottom wall, including the vertical segment located at the drop-off, is kept at constant temperature T_{hot}. The inlet and outlet conditions remain the same as before.

To keep a similar theme going, the three cases simulated on this geometry correspond to a Rayleigh number of 3000 and Reynolds numbers of 0.1, 20, and 54. The characteristic length is taken to be the full expanded width of the channel downstream, which means the Rayleigh number is significantly smaller (well below critical value) in the initial narrow section of the channel. This implies that convection cells cannot form within it, as will be seen in Figure 9.

The sudden-expansion channel data for $Re = 0.1$ is shown below in Figures 9 and 10, $Re = 20$ shown in Figures 11 and 12, and $Re = 54$ shown in Figures 13 and 14. The lattice grid size, as well as all key parameters, share the same values as their uniform-width geometry counterparts that were modeled previously at the same Rayleigh-Reynolds combinations.
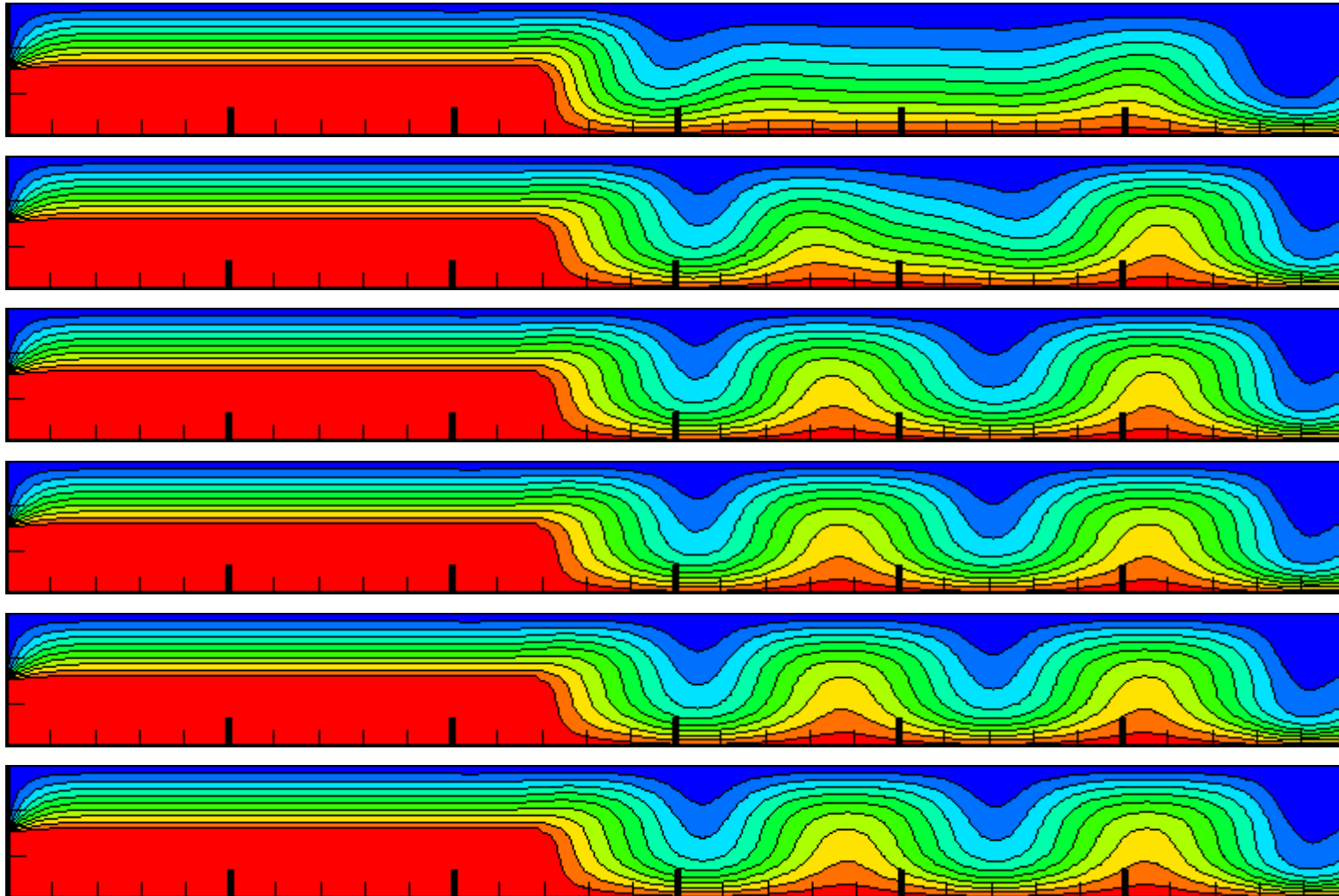
Figure 9 Expanded-channel temperature contours for Re = 0.1, $Ra = 3000$

at time steps 1000, 2000, 3000, 4000, 5000, and 6000
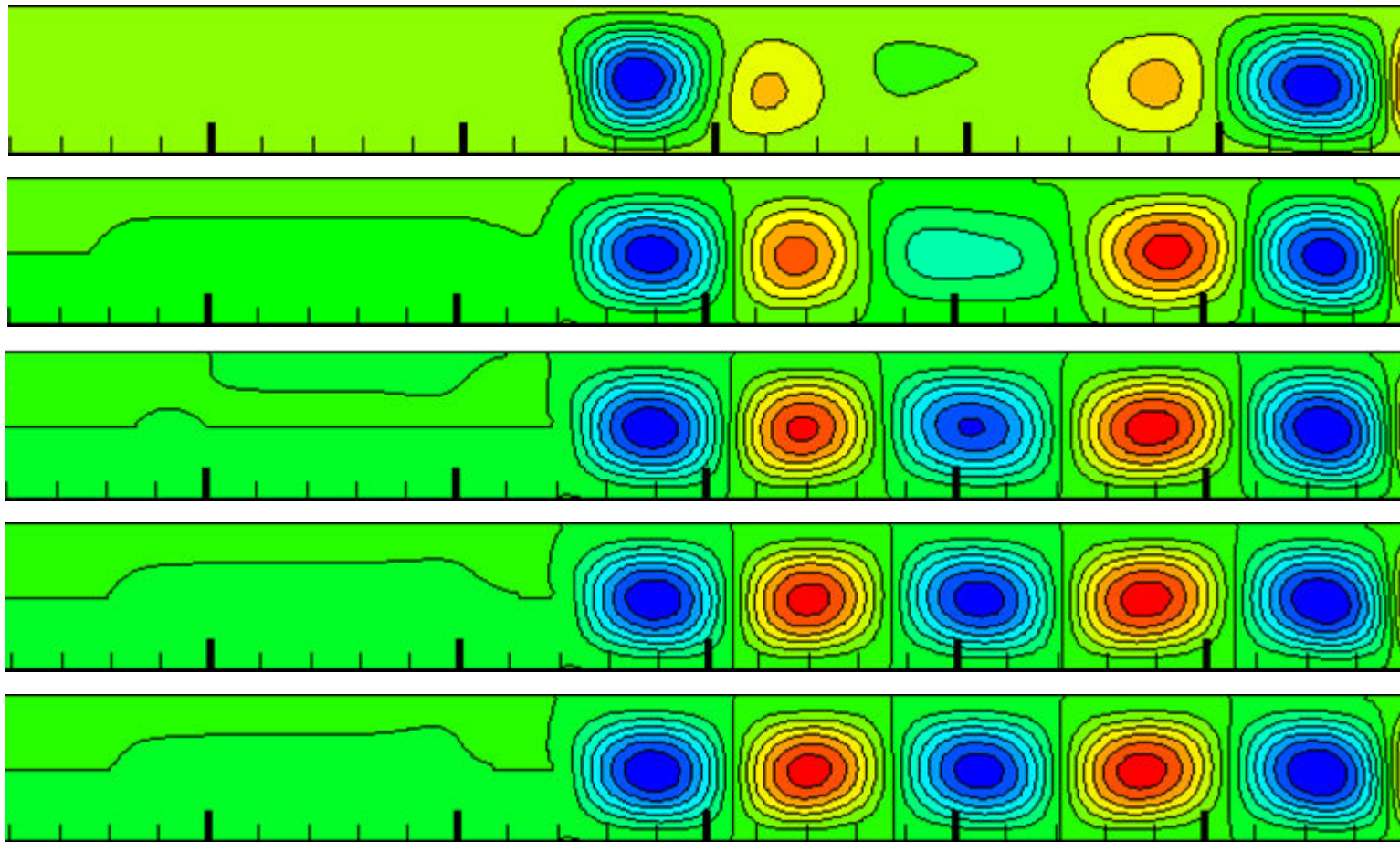
Figure 10 Expanded-channel stream function contours for Re = 0.1, Ra = 3000
at time steps 1000, 2000, 3000, 4000, and 5000
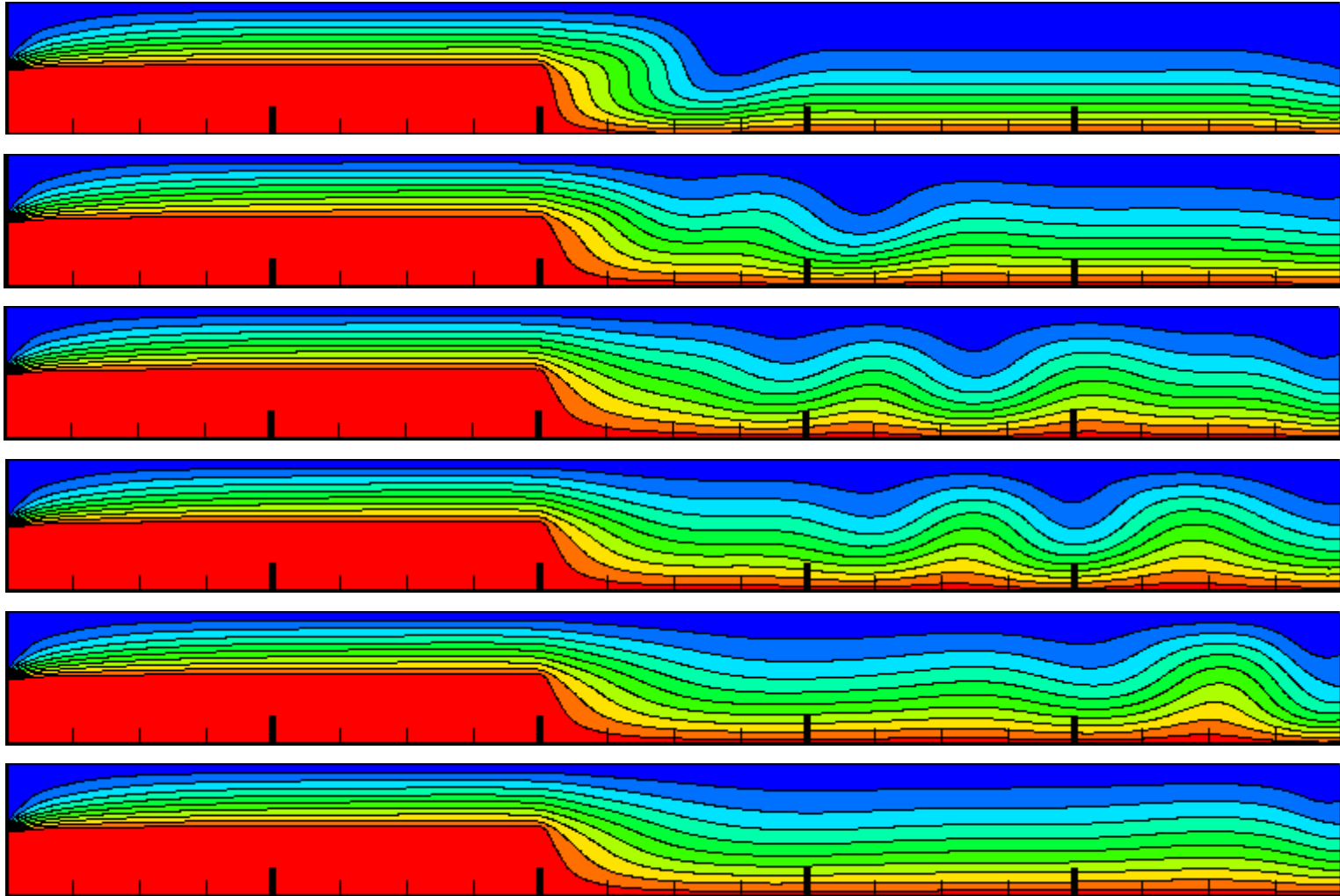
Figure 11 Expanded-channel temperature contours for Re $= 20$, $Ra = 3000$

at time steps 3000, 5000, 8000, 10000, 20000, and 50000

36
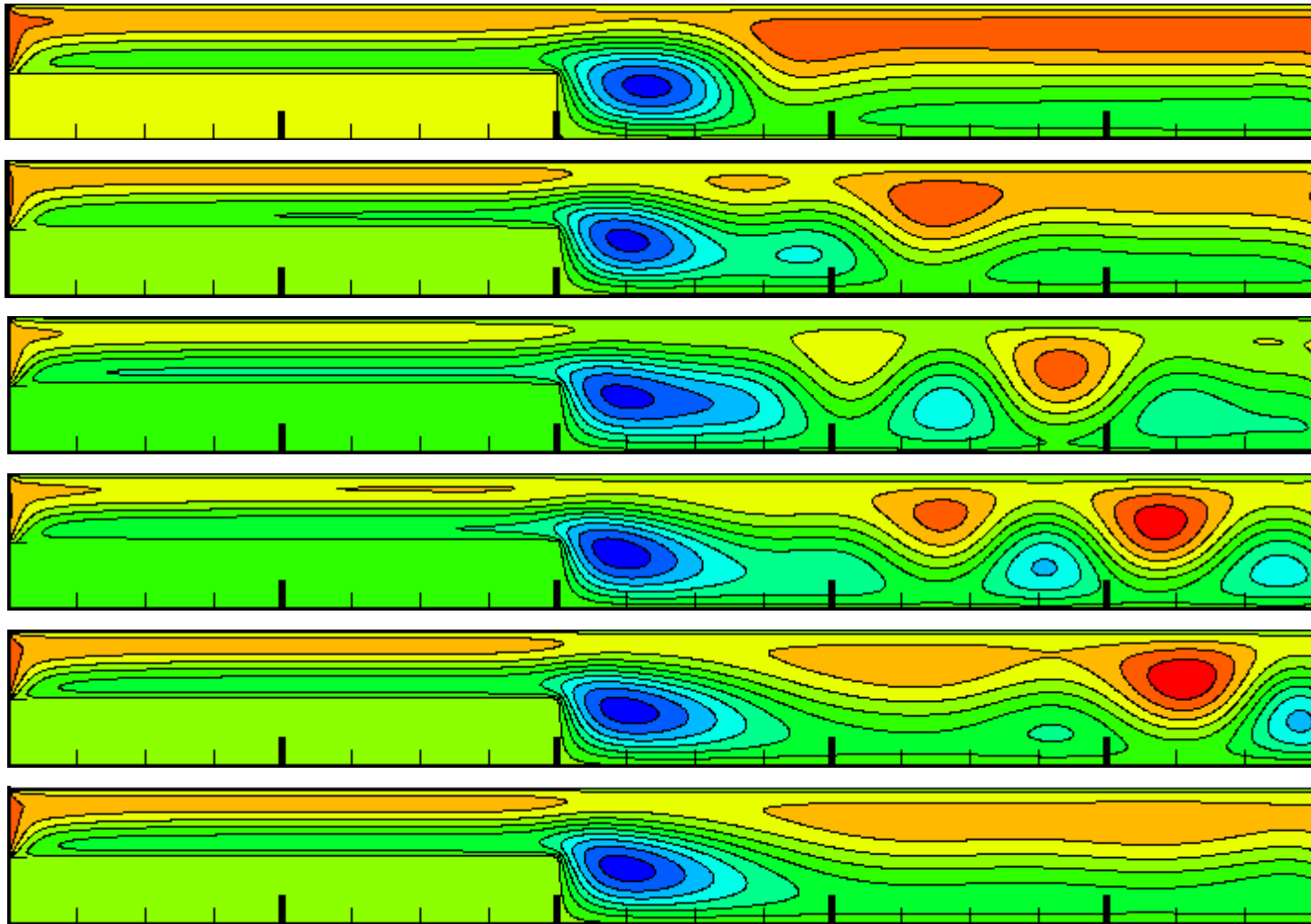
Figure 12 Expanded-channel stream function contours for Re $= 20$, $Ra = 3000$

at time steps 3000, 5000, 8000, 10000, 20000, and 50000

37
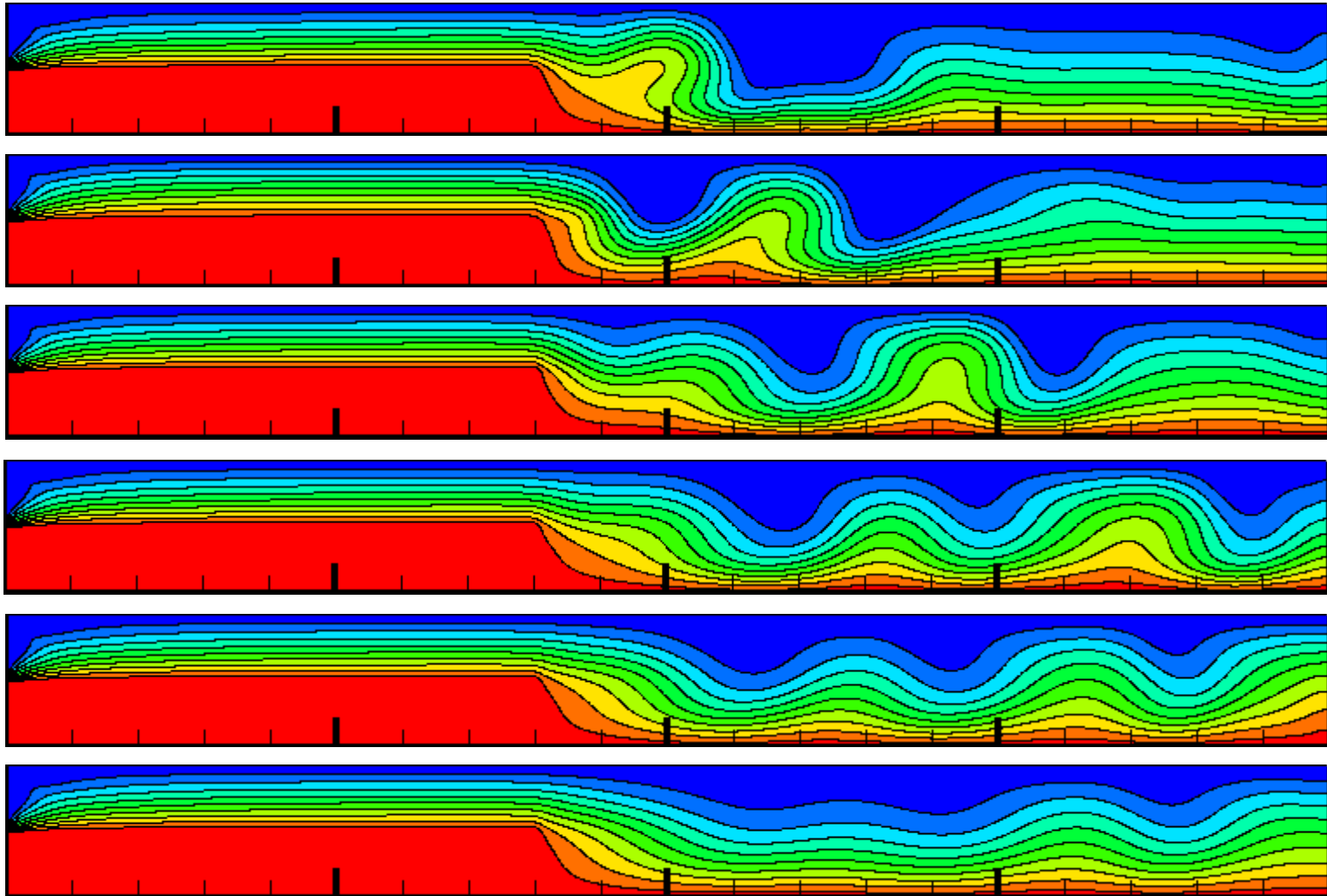
Figure 13 Expanded-channel temperature contours for Re $= 54$, $Ra = 3000$

at time steps 15000, 20000, 30000, 40000, 50000, and 75000
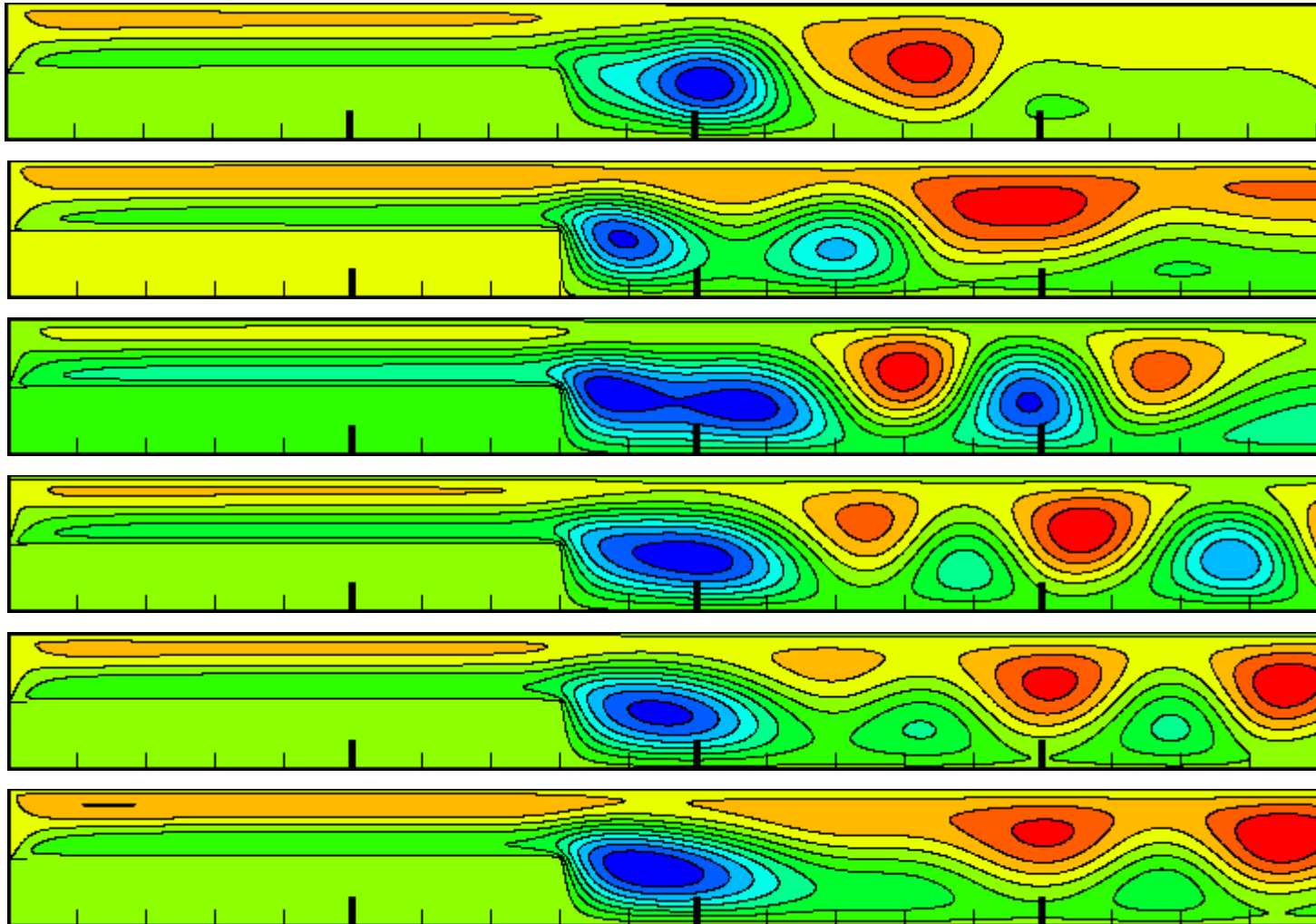
Figure 14 Expanded-channel stream function contours for Re $= 54$, $Ra = 3000$

at time steps 15000, 20000, 30000, 40000, 50000, and 75000

39

Channel with Sudden Contraction

The final geometry examined here is a channel undergoing sudden contraction at a location 60% downstream. The heated bottom wall sharply rises and constricts the channel to half of its original width. Boundaries are treated the in the same fashion as those for the sudden-expansion channel. The characteristic length is once again the width of the widest section of channel, so the Rayleigh number in the constricted section of channel near the outlet is well below critical value and similarly does not allow formation of convection cells there.

Lattice dimensions and simulation parameters are still the same values as their corresponding Rayleigh-Reynolds combinations shown for the previous geometries. See Figures 15 and 16 for $Re = 0.1$ data, and Figures 17 and 18 for $Re = 20$ data, both for the contracted channel.
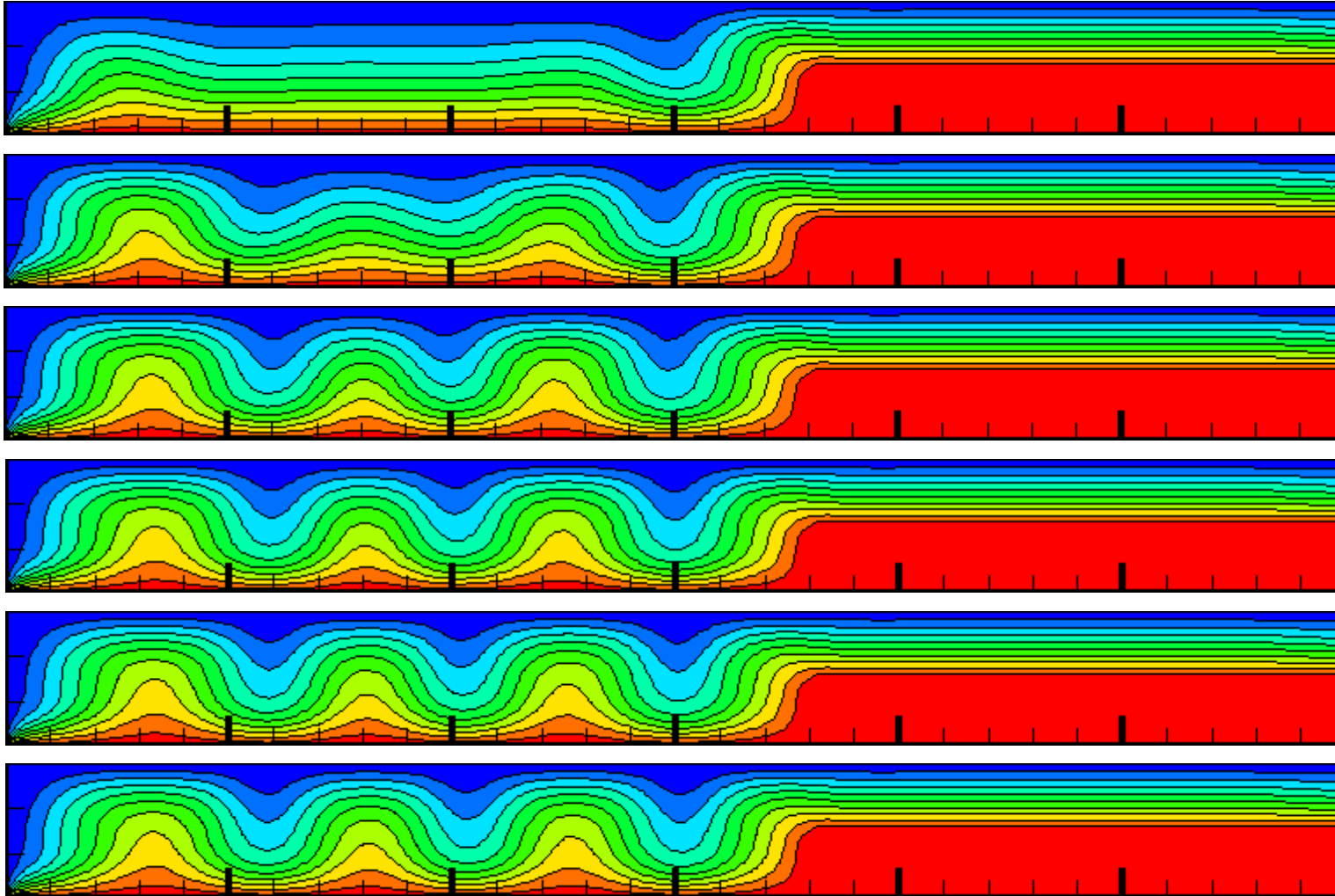
Figure 15 Contracted-channel temperature contours for Re $= 0.1$, $Ra = 3000$

at time steps 1000, 2000, 3000, 4000, 5000, and 6000
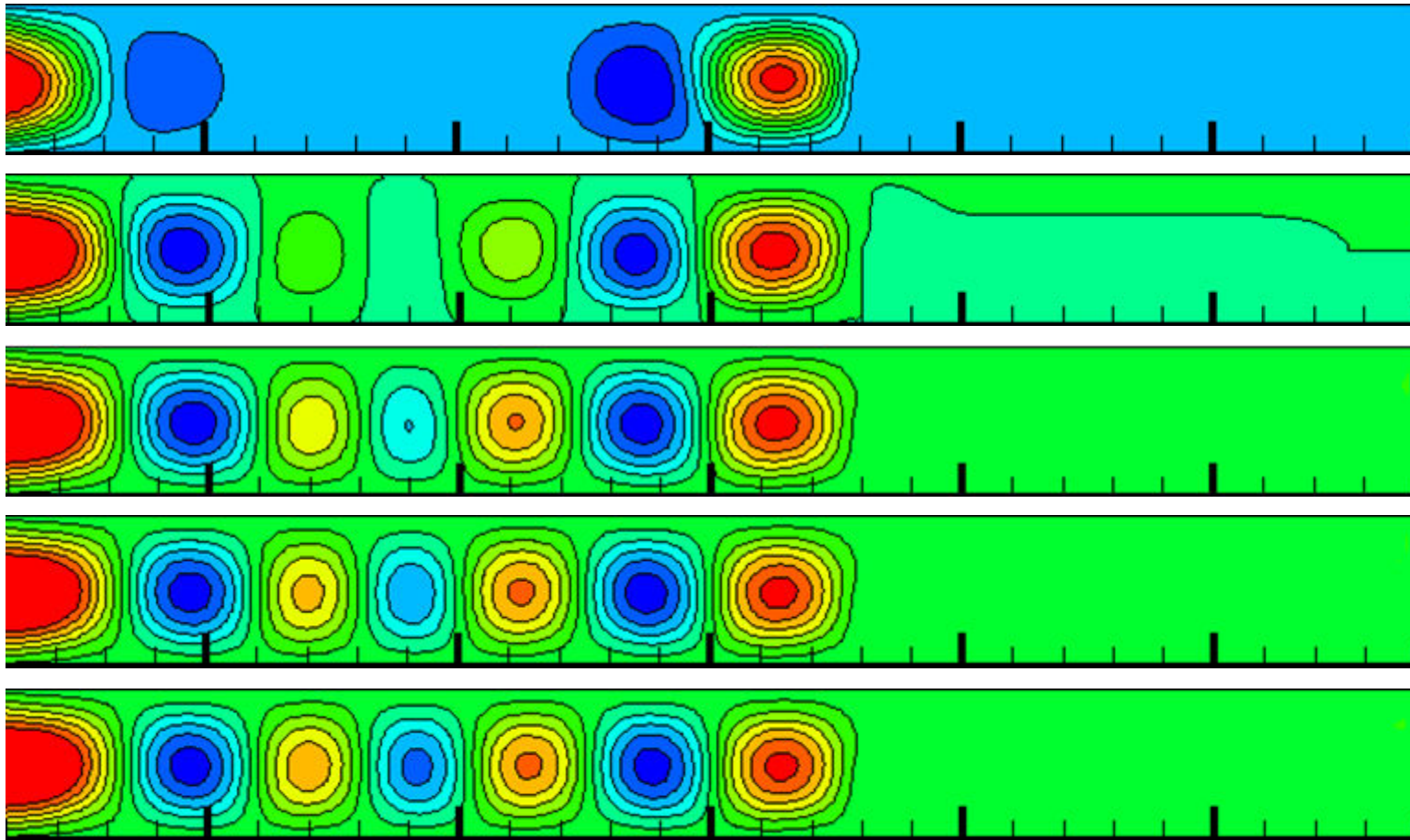
Figure 16 Contracted-channel stream function contours for Re = 0.1, $Ra = 3000$

at time steps 1000, 2000, 3000, 4000, and 5000
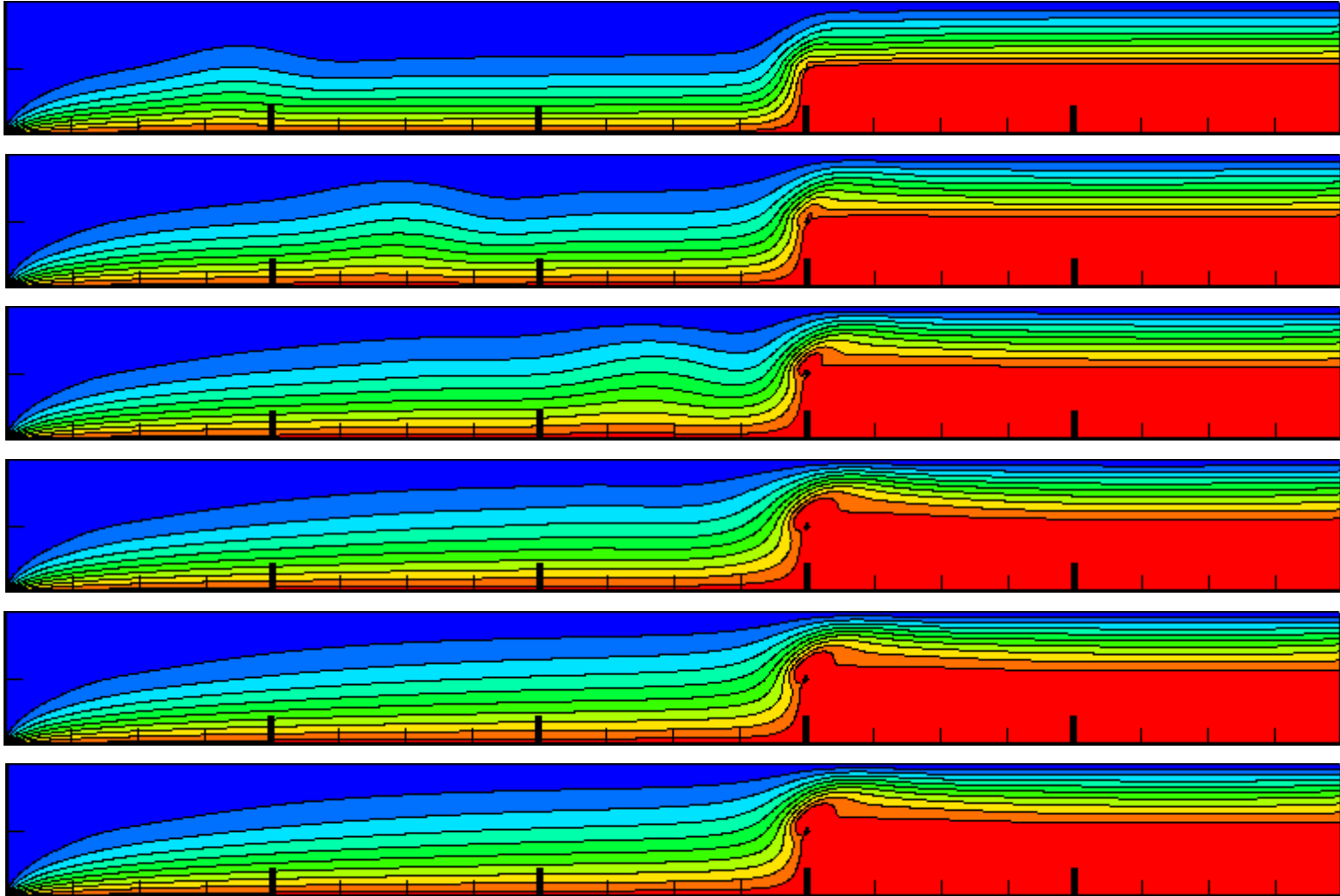
Figure 17 Contracted-channel temperature contours for Re $= 20$, $Ra = 3000$

at time steps 3000, 5000, 8000, 10000, 20000, and 50000
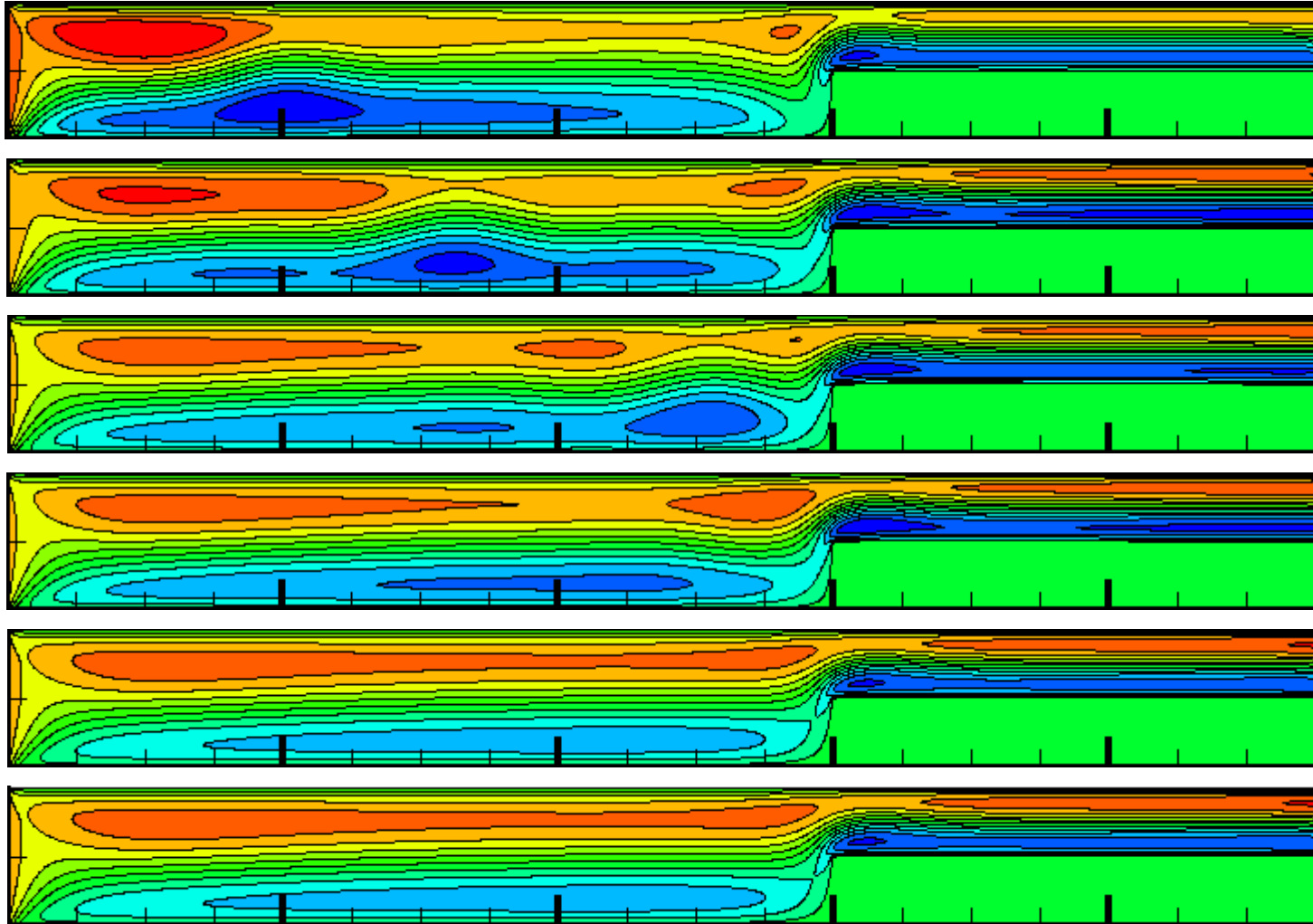
Figure 18 Contracted-channel stream function contours for Re = 20, $Ra = 3000$
at time steps 3000, 5000, 8000, 10000, 20000, and 50000

44

Conclusion

The Lattice Boltzmann method, extended to simulate both hydrodynamic motion and heat transfer, has proven to be a powerful and versatile modeling tool. Trials performed against accepted elementary flows were shown to be accurate within about 1% error on relatively small grid sizes. As illustrated here, thermal LBM can effectively capture the behaviors of both natural and forced convection in action. Fairly simple methods for applying hydrodynamic and thermal boundary conditions prove to be sufficient for all common situations. Relations to physical properties are also determinable if desired.

There are certainly opportunities to further build on this research, as LBM has many more capabilities to improve stability and versatility. Additional techniques include a multi-relaxation-time scheme to aid in stability, extension to three-dimensional space, conditions for curved and membrane boundaries, evolution and interaction for multiphase scenarios, an entropic method for high-Reynolds flows, and much more.

References

Abe, T. "Derivation of the Lattice Boltzmann Method by Means of the Discrete Ordinate Method for the Boltzmann Equation." *Journal of Computational Physics* 131 (1997): 241.

Alexander, F. J., S. Chen, and J. D. Sterling. "Lattice Boltzmann Thermohydrodynamics." *Physical Review E* 47 (1993): R2249.

Bartolini, A., C. Battista, S. Cabasino, et al. "LBE Simulation of Rayleigh-Bénard Convection on the APE100 Parallel Processor." *International Journal of Modern Physics C* 4 (1993): 993.

Bhatnagar, P. L., E. P. Gross, and M. Krook. "A Model for Collision Process in Gases. I. Small Amplitude Processes in Charged and Neutral One-component System." *Physical Review* 94.3 (1954): 511-25.

Eggels, J. G. M., and J. A. Somers. "Numerical Simulation of Free Convective Flow Using the Lattice Boltzmann Scheme." *Journal of Heat and Fluid Flow* 16 (1995): 357.

Hardy, J., O. De Pazzis, and Y. Pomeau. "Molecular Dynamics of a Classical Lattice Gas: Transport Properties and Time Correlation Functions." *Physical Review A* 13.5 (1976): 1949-961.

He., X., and L. Luo. "A Priori Derivation of the Lattice Boltzmann Equation." *Physical Review E* 55 (1997 a): R6333.

He., X., and L. Luo. "Lattice Boltzmann Model for the Incompressible Navier-Stokes Equation." *Journal of Computational Physics* 88.3/4 (1997 b): 927-44.

He., X., S. Chen, and G. D. Doolen. "A Novel Thermal Model for the Lattice Boltzmann Method in Incompressible Limit." *Journal of Computational Physics* 146 (1998): 282-300.

Hou, S., Q. Zou, S. Chen, G. D. Doolen, and A. Cogley. "Simulation of Cavity Flow by the Lattice Boltzmann Method." *Journal of Computational Physics* 129 (1995): 329.

Latt, Jonas. "Choice of Units in Lattice Boltzmann Simulations." Technical report for LBMethod.org. 2008.

Liu, C., K. Lin, H. Mai, and C. Lin. "Thermal Boundary Conditions for Thermal Lattice Boltzmann Simulations." *Computers and Mathematics with Applications* 59.7 (2010): 2178-93.

Llewellin, E. W. "LBflow: An Extensible Lattice Boltzmann Framework for the Simulation of Geophysical Flows. Part I: Theory and Implementation." *Computers & Geosciences* 36.2 (2010):115-22.

Martínez, D. O., W. H. Matthaeus, S. Chen, and D. C. Montgomery. "Comparison of

Spectral Method and Lattice Boltzmann Simulations of Two-dimensional

Hydrodynamics." *Physics of Fluids* 6.3 (1994): 1285.

McNamara, G., A. L. Garcia, and B. J. Alder. "Stabilization of Thermal Lattice

Boltzmann Models." *Journal of Statistical Physics* 81 (1995): 395.

Shan, X. "Solution of Rayleigh-Bénard Convection Using a Lattice Boltzmann Method."

Physical Review E 55 (1997): 2780.

Succi, Sauro. *The Lattice Boltzmann Equation for Fluid Dynamics and Beyond*. Oxford:

Clarendon, 2001.

Succi, Sauro, Roberto Benzi, and Francisco Higuera. "The Lattice Boltzmann Equation:

A New Tool for Computational Fluid-dynamics." *Physica D: Nonlinear*

Phenomena 47.1-2 (1991): 219-30.

Zou, Q., and X. He. "On Pressure and Velocity Boundary Conditions for the Lattice

Boltzmann BGK Model." *Physics of Fluids* 9.6 (1997): 1591.

Vita

Gregory A. Scott was born in Allentown, Pennsylvania in 1991. He is the oldest son of Gary and Ruby Scott, who immersed him in nearby Lehigh University's culture right from birth. After graduating from Southern Lehigh High School in 2009, Greg attended Lehigh University for his Bachelor of Science degree in Mechanical Engineering with a minor in Aerospace Engineering. He graduated in 2013 and made a late decision to remain at Lehigh and pursue a Master of Engineering degree in the same major. In the spring of 2014 Greg was invited by his advisor Dr. Alparslan Oztekin to join Lehigh's Lattice Boltzmann research team, and suddenly found himself now advancing towards a Master of Science degree. He now looks forward to continuing his studies at Lehigh to earn a PhD in Mechanical Engineering, beyond his original academic plans, but looking forward to the challenge nonetheless.